Graduate School ETD Form 9
(Revised 01/14)

PURDUE UNIVERSITY
GRADUATE SCHOOL
Thesis/Dissertation Acceptance

This is to certify that the thesis/dissertation prepared

By Margaret Mary Brass

Entitled

BIOMECHANICAL AND MORPHOLOGICAL CHARACTERIZATION OF COMMON ILIAC VEIN REMODELING: EFFECTS OF VENOUS REFLUX AND HYPERTENSION

For the degree of Master of Science in Biomedical Engineering

Is approved by the final examining committee:

Ghassan S. Kassab

Sungsoo Na

Edward J. Berbari

To the best of my knowledge and as understood by the student in the *Thesis/Dissertation Agreement. Publication Delay, and Certification/Disclaimer (Graduate School Form 32)*, this thesis/dissertation adheres to the provisions of Purdue University's "Policy on Integrity in Research" and the use of copyrighted material.

Approved by Major Professor(s): Ghassan S. Kassab

Approved by: Edward J. Berbari 04/11/2014

Head of the Department Graduate Program Date

BIOMECHANICAL AND MORPHOLOGICAL CHARACTERIZATION OF COMMON ILIAC VEIN REMODELING: EFFECTS OF VENOUS REFLUX AND HYPERTENSION

A Thesis

Submitted to the Faculty

of

Purdue University

by

Margaret Mary Brass

In Partial Fulfillment of the

Requirements for the Degree

of

Master of Science in Biomedical Engineering

May 2014

Purdue University

Indianapolis, Indiana

ACKNOWLEDGMENTS

I would like to express the deepest appreciation to my thesis advisor, Dr. Ghassan Kassab, for his assistance, guidance, and supervision during the entire course of this research and thesis work. Dr. Ghassan Kassab generously shared his passion and wisdom for research with me and I am very thankful to have been a part of his lab.

I would like to thank my advisory committee members, Dr. Edward Berbari and Dr. Sungsoo Na, for their time and insight during the completion of this thesis.

I would like to express my gratitude to Dr. Zachary Berwick and Dr. Mark Svendsen, for all their help, valuable contributions, and insightful discussions that led to the successful completion of this research and thesis. Without their guidance and persistent help this thesis would not have been possible.

I thank Dr. Zachary Berwick and Mr. Joshua Krieger for permission to include the large animal model within this thesis. I have greatly benefited from working with them both and greatly appreciate the feedback and support they have offered throughout my research and thesis work.

Special thanks to Dr. Huan Chen. Without her help and guidance, the multiphoton microscopy done in this thesis would not have materialized. For that I owe my deepest gratitude to her.

I would also like to thank my co-workers, especially Dr. Jenny Choy, Dr. Xiao Lu, Dr. Xiaomei Guo, and Dr. Xuefeng Zhao. The knowledge each of them has bestowed upon me is invaluable. My deepest appreciation goes to Ms. Valerie Lim Diemer for her assistance in formatting this thesis.

TABLE OF CONTENTS

Page

Page

LIST OF FIGURES

SYMBOLS

λ_{phys}	physiologic stretch ratio
Φ_o	open angle
R_{in}	zero stress condition inner radius
R_{out}	zero stress condition outer radius
L_{in}	inner arc length
L_{out}	outer arc length
T	zero stress condition thickness
r_{in}	loaded condition inner radius
r_{out}	loaded condition outer radius
λ_z	axial stretch ratio
λ_θ	circumferential stretch ratio
λ_r	radial stretch ratio
L	axial length at unloaded condition
l	axial length at loaded condition
χ	non-dimensional scaling condition
$r_{average}$	loaded condition average radius
E_{zz}	axial Green strain
$E_{\theta\theta}$	circumferential Green strain
P	pressure
F	force
σ_z	axial Cauchy stress
σ_θ	circumferential Cauchy stress
S_z	axial Kirchhoff stress
S_θ	circumferential Kirchhoff stress

W	Fung-type SEF
α_1	non-dimensional proportionality constant in circumferential direction
α_2	non-dimensional proportionality constant in axial direction
α_4	non-dimensional constant for cross talk between circumferential and axial direction
C	stress scaling factor
r	nonlinear correlation coefficient

ABBREVIATIONS

CSA	cross sectional area
DVT	deep vein thrombosis
ECG	electrocardiogram
ECM	extracellular matrix
ECs	endothelial cells
EGTA	ethylene glycol tetraacetic acid
FVP	femoral venous pressure
IVUS	intravascular ultrasound
JVP	jugular venous pressure
KCl	potassium chloride
LCI	left common iliac
MPM	multiphoton microscopy
NIH	National Institutes of Health
PBS	phosphate buffer solution
PMT	photomultiplier tube
PTS	post-thrombosis syndrome
PWV	pulse wave velocity
RAP	right atrial pressure
RCI	right common iliac
RVP	right ventricle pressure
SD	standard deviation
SE	standard error
SEF	strain energy function
SHG	second-harmonic generation

TPEF	two-photon excited fluorescence
VSMCs	vascular smooth muscle cells

ABSTRACT

Brass, Margaret Mary. M.S.B.M.E., Purdue University, May 2014. Biomechanical and Morphological Characterization of Common Iliac Vein Remodeling: Effects of Venous Reflux and Hypertension. Major Professor: Ghassan Kassab.

The passive properties of the venous wall are important in the development of venous pathology. Increase in venous pressure due to retrograde flow (reflux) and obstruction of venous flow by intrinsic and extrinsic means are the two possible mechanisms for venous hypertension. Reflux is the prevailing theory in the etiology of venous insufficiency. The objective of this thesis is to quantify the passive biomechanical response and structural remodeling of veins subjected to chronic venous reflux and hypertension. To investigate the effects of venous reflux on venous mechanics, the tricuspid valve was injured chronically in canines by disrupting the chordae tendineae. The conventional inflation-extension protocol in conjunction with intravascular ultrasound (IVUS) was utilized to investigate the passive biomechanical response of both control common iliac veins (from 9 dogs) and common iliac veins subjected to chronic venous reflux and hypertension (from 9 dogs). The change in thickness and constituent composition as a result of chronic venous reflux and hypertension was quantified using multiphoton microscopy (MPM) and histological evaluation. Biomechanical results indicate that the veins stiffened and became less compliant when exposed to eight weeks of chronic venous reflux and hypertension. The mechanical stiffening was found to be a result of a significant increase in wall thickness ($p < 0.05$) and a significant increase in the collagen to elastin ratio ($p < 0.05$). After eight weeks of chronic reflux, the circumferential Cauchy stress significantly reduced ($p < 0.05$) due to wall thickening, but was not restored to control

levels. This provided a useful model for development and further analysis of chronic venous insufficiency and assessment of possible intervention strategies.

1. INTRODUCTION

1.1 Anatomy of the Healthy Venous System

The circulation of blood is a closed loop circuit which is comprised of a high pressure arterial system and a low pressure venous system. The arterial and venous systems are connected through microscopic exchange vessels called capillaries. Arteries and veins are the conduits that transport blood to and from tissues located throughout the body. [1]. The primary function of the arterial system is to deliver oxygen-rich blood to the body, while the primary function of the venous system is to return deoxygenated blood to the heart [2]. Deoxygenated blood within the systemic circulation may return to the heart through three pathways: the coronary sinus, the superior vena cava, and the inferior vena cava.

The deoxygenated blood from the veins of the lower extremities (i.e. the legs), which are the primary focus of this thesis, return to the heart through the inferior vena cava. The veins of the lower limbs are divided into three subcategories: the superficial veins, the deep veins, and the perforating veins [3]. The superficial veins lie above the fibrous tissue enclosing the muscles of the leg (muscular fascia) and drain the micro-vessels located between the skin and deep muscular fascia; while the deep veins lie beneath the muscular fascia and serve as the primary collecting veins. The perforating veins, located in the thigh and lower leg, connect the superficial veins to the deep veins. The deep veins then allow for the blood in the lower extremities to be drained into the inferior vena cava and returned to the heart.

Figure 1.1 depicts the major veins of the lower extremities. Venous blood from the superficial veins and the deep calf veins drain into the femoral vein. The femoral vein converges with the common iliac vein and the common iliac veins drains the venous

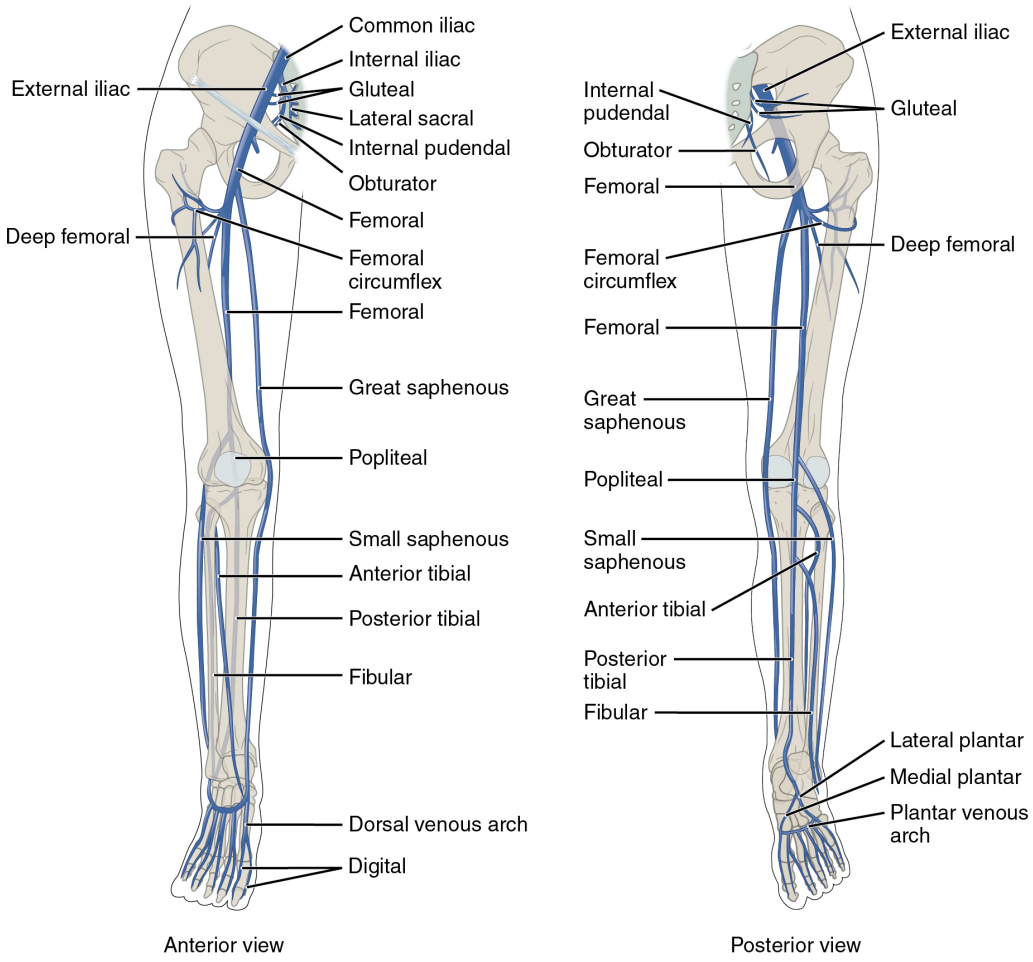

Fig. 1.1. Anterior and posterior views showing the major veins of the lower extremities that drain into the inferior vena cava [1].

blood from the lower extremities into the inferior vena cava [4]. The vessel studied throughout this thesis is the common iliac vein.

1.1.1 Mechanisms of Venous Return

The volume of blood which returns to the heart is referred to as venous return. In the upper extremities, gravity serves as a mechanism of venous return to the heart. However, in the lower extremities, gravity causes the blood to accumulate when in the

standing posture. The accumulation created by gravity is a deterrent of venous return. Under normal circumstances, the pressure at the venous end of the capillaries is between 12 and 18 mmHg [5]. Gravity, when standing, can cause blood to accumulate and the venous pressure in the lower extremities to significantly rise. This increase is due to the fact that venous pressure is determined by two components: a hydrostatic component and a hydrodynamic component [6]. The hydrostatic component of venous pressure is a result of gravitational forces and is related to the weight of the column of the blood [7]. The hydrodynamic component, on the other hand, is not related to gravity, but to the pressure generated by the contraction of the skeletal muscles of the leg [6]. In summary, the hydrostatic component of pressure is responsible for the increase in venous pressure when standing [8].

Dividing the hydrostatic column into segments prevents an increase in venous pressure. A series of bicuspid (two leaflets) valves are located throughout the deep and superficial veins which divide the hydrostatic column of blood into segments [9]. In addition to the venous valves, the veins of the lower extremities are surrounded by muscles. These muscles serve as pumps. When they contract the blood is propelled within the veins towards the heart. The muscle pump in conjunction with the one way venous valves permit blood flow towards the heart and prevent retrograde flow. These two mechanisms of venous return lead to an emptying of the deep and superficial veins and a fall in overall venous pressure [6].

1.1.2 Structure of the Vein

As summarized above, the venous system is a low pressure system whose primary function is to return the venous blood to the heart, using a system of valves and a muscle pump. Despite the functional differences of arteries and veins, all major blood vessels consist of three primary layers: the intima, the media, and the adventitia. Figure 1.2 illustrates the structural similarities and differences of the arteries and veins.

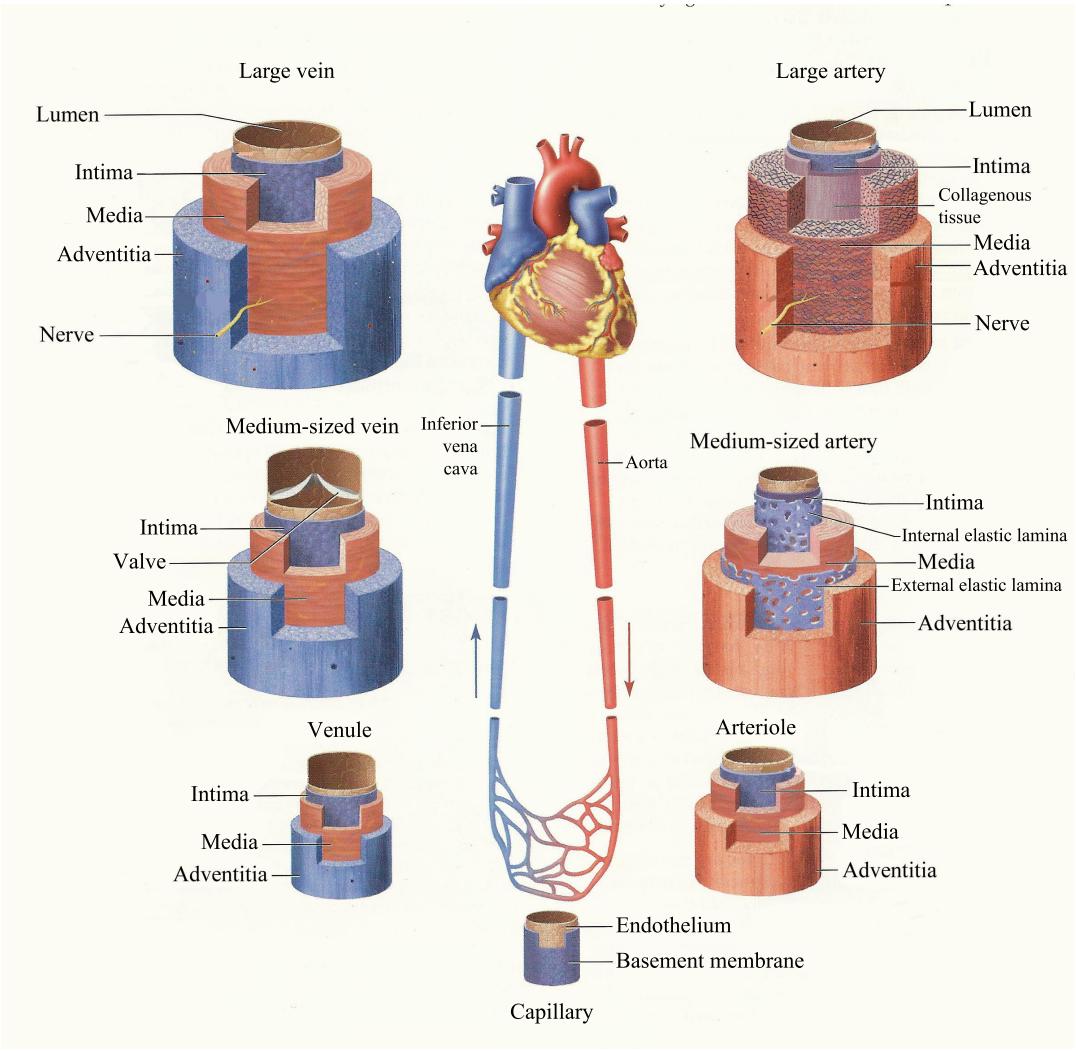

Fig. 1.2. Illustration of the structure of arteries and veins [1].

The main constituents that make up the layers of both the arterial and venous wall are endothelial cells (ECs), collagen, elastin, vascular smooth muscle cells (VSMCs), and ground substances. Due to the lower pressures seen in veins, the configuration of the five main constituents within each layer of the vein differs from that of the artery [10]. The venous intima consists of a thin continuous monolayer of ECs laying on the basal lamina. However, a clearly defined intima only exists in large veins because the intima of large veins may also contain a thin band of connective tissue beneath the endothelial basal lamina [11].

The media layer of the vein is relatively thin. However, it contributes to the vessel properties more significantly than the intima or the adventitia do [12]. The media is composed of one or more layers of VSMCs interspersed with collagen, elastin, and ground substances [11]. The layer(s) of VSMCs are circumferentially oriented and allows the vein to constrict and dilate in response to pressure [13]. Circumferentially aligned collagen is the predominate component of the extracellular matrix (ECM) of the media [14] and prevents the vein from excessive dilation [13]. Media elastin allows for the vein to expand with pressure in order to maintain adequate blood flow; however, elastin is scare in the medial layer of veins [13]. Lastly, the adventitia is the outermost layer of the vein and is the thickest of the three layers in the healthy vein. It consists mostly of circumferentially oriented collagen interspersed with bands of elastin fibers [11].

The predominant structural differences between the veins and arteries are the significant absence of elastin in the media and the overall thickness of the vessel wall [15, 16]. The arterial wall contains more VSMCs and elastin than the venous wall and is thicker than the corresponding venous wall. However, the veins thinner walls contain a larger amount of inextensible collagen [15]. Despite the larger amounts of inextensible collagen and lower amounts of VSMCs and elastin, the venous wall is more distensible than the arterial wall. This indicates that the thinness of the venous wall promotes higher distensibility of the veins more significantly than the ratio of collagen and elastin [13].

1.2 Chronic Venous Insufficiency

Beebe et al. found that Chronic Venous Insufficiency (CVI) can compromise the strength of the vein wall by altering the collagen and elastin content [4]. CVI is a condition that effects the venous system of the lower extremities with venous hypertension causing various sequelae including pain, swelling, edema, skin changes, and ulceration [3, 17]. CVI affects 10 to 35% of the adult population in the United

States [18]. Annually, 1 to 3% of the total health care budget is spent on CVI related treatment [7]. The socioeconomic impact of venous ulceration is dramatic. Venous ulceration impairs an individuals ability to engage in social and occupational activities. This impairment not only impacts the patients quality of life but imposes financial constraints [3], ∼2 million work days are lost annually in the United States [19].

Reflux (venous retrograde flow) due to venous valve incompetence is the prevailing theory in the etiology of venous hypertension [4, 6, 20, 21]. Venous hypertension is primarily due to incompetent valves, but secondary causes are obstruction of venous outflow, or failure of the muscle pump [22]. Venous hypertension depends upon the hydrostatic and hydrodynamic pressure components. When valve failure occurs, the venous pressure in surrounding tissue and capillaries rises. Increased venous hydrostatic pressure causes a shift in the venous hemodynamics with changes in wall shear stress [23]. This initiates the inflammatory cascade [24]. Pascarella et al. reported that the inflammatory response increases as the reflux rate increases [24]. Pathologic changes in the valves and venous wall are linked to venous hypertension and leukocyte infiltration and activation [7].

Venous reflux through incompetent venous valves is the primary cause of the venous hypertension that underlies the clinical manifestations of CVI [3, 25]. Pascarella et al. and Dalsing et al. have both developed animal models of venous insufficiency [24, 26]. Pascarella et al. created a rat model of venous insufficiency by constructing a femoral arteriovenous fistula [24], while Dalsing et al. developed a canine model of venous insufficiency by disrupting the venous valves of the hind limb [26].

Pascarella et al. reported that the formation of the arteriovenous fistula produced an immediate ∼10-fold increase in venous pressure (96 mmHg vs. 9 mmHg) and dilation of the distal veins. Detectable reflux flow was not immediately observed and was not substantially detected until several days post-surgery. The increased reflux mirrored progressive changes in the venous valve morphology. Bergan et al. reported

that this model demonstrates that prolonged venous hypertension leads to valvular incompetence and eventually complete cusp destruction [25]. Histology showed that thickening and fibrosis of the venous wall became present after 3 weeks [24]. Pascarella et al. findings indicate that the inflammation cascade was initiated as a result of the venous hypertension. The ∼10-fold increase in venous pressure obtained in this model is a major pressure increase due to reflux. This is a result of the arteriovenous fistula and the introduction of arterial pressures and flow. However, increases of that magnitude do not mimic the natural reflux in the low pressure venous system. There exists a need for a model which mimics the hemodynamic conditions associated with venous reflux more accurately.

Dalsing et al. disrupted the venous valves of the hind limb by introducing a vavulotome. This model allows for short-term studies of venous insufficiency to be conducted in the anesthetized up-right position. Significant reflux was only observed when the animals were in the up-right position or walking on their hind limbs. Even after the venous valves were disrupted, normal hemodynamic measurements were recorded during quadruped walking. Unlike humans, canines do not exhibit a large hydrostatic pressure in their lower limbs. Therefore, disruption of the venous valves does not affect a quadruped as significantly as it would a biped unless the animal is forced to act as a biped [26]. Thus, this is a conditional model, since in the animals normal anatomical position, hemodynamic changes from baseline were not observed. No current animal model mimics the human ability to walk upright [27]. Therefore, there exists a need for an animal model which induces venous reflux in the animals normal anatomical position (on all four legs). Lastly, no biomechanical tests have been performed on the veins of either model [24–26]. No data exists on the passive biomechanical response of venous tissue subjected to chronic venous hypertension due to reflux.

1.2.1 Venous Hypertension

Venous hypertension causes the various sequelae associated with CVI [3]. Hypertension is defined as abnormally elevated blood pressure. It has been well documented through experimental studies and clinical observations that arteries remodel as a consequence of increased wall stress due to chronic arterial hypertension [28]. Watts et al. reported that the remodeling seen in arteries includes a reorganization of the structural support provided by the extracellular matrix as well as wall hypertrophy [29]. Wall hypertrophy, the thickening of the vessel wall, is the primary biomechanical phenomenon that occurs in response to arterial hypertension. Thickening of the arterial wall restores the circumferential Cauchy wall stress to a normal, control level, but it also creates an arterial wall that is thicker and less compliant [29].

Unlike arteries, there is a dearth of information related to the effects of chronic venous hypertension upon venous wall mechanics [30]. Venous hypertension can be induced by vessel constriction [31], gravitational loading [8, 32, 33], volume overload [29], and arteriovenous fistulas [24]. Monos et al. and Watt et al. both have reported that the wall thickness of the vein does not change when venous hypertension is induced [8, 29, 32, 33]. Monos et al. results did show that the external diameters were larger in the hypertensive animals than the control animals when compared at the same pressure. Although Monos et al. did not observe wall thickening, the wall still was found to be stiffer in the hypertensive animals. Contradictory to Monos et al. and Watt et al., Hayashi et al. reported a significant increase in wall thickness as soon as one week after hypertension was created. This increase in wall thickness was found to restore circumferential Cauchy wall stress to the control level [31]. In later studies, Hayashi et al. reported that the remodeling phenomena observed in the femoral vein due to hypertension was similar to those observed in hypertensive arteries [30]. Hayashi et al. concluded that when the vein is chronically exposed to a 2-fold increase in blood pressure, due to vessel constriction, circumferential wall stress is rapidly restored to the control level due to wall thickening and structural

remodeling. Choy et al. also observed that the coronary vein transformed from a thin-walled, large lumen vessel to a thick-walled, smaller lumen vessel in response to elevated pressures [34, 35]. The increase in thickness was found to decrease the circumferential Cauchy stress.

There is no consensus on how the venous wall reacts to chronic venous hypertension. The current literature reports that venous stiffness and thickness increases, decreases, and remains the same with hypertension. This may be due to the inherent differences between the various animal models, vessels studied, and periods of development of hypertension.

The remodeling phenomena observed in vein grafts are much different from those seen in the veins in hypertension models induced by gravitational loads or vessel compression. As veins are introduced into the arterial system for use as a bypass graft they undergo a significant change in biomechanical environment. Severyn et al. reported increases in intraluminal pressure, blood flow and cyclic loading due to pulsatility [36]. Monos et al. reported that the wall thickness of the vein graft increases substantially within a few days and rearrangement of the structure occurs [37]. Owens et al. used standard duplex to surveillance the lumen diameter and pulse wave velocity (PWV) of lower venous grafts implanted in humans. Results showed that a 65% increase in overall stiffness of the vein graft wall occurred during the first six months after implantation. However, the stiffness did not change significantly during the first month post implantation of the graft [38]. Dobrin et al. observed, after three months, canine vein grafts dilated in absolute size, but retained distensible at low pressure and virtually indispensable at pressures above 35-50 mmHg [39].

Intimal hyperplasia and medial thickening are the two structural changes which occur in vein grafts [39]. Dorbin et al. concluded that the intimal hyperplasia and medial thickening are the results of two different stimuli. The intimal hyperplasia may result from abnormal flow characteristics at the blood-intima interface, while the medial thickening is likely due to the arterial pressure [39]. Again, there is an inherent difference between the various animal models, vessels studied, and periods

of development of hypertension. However, studies on vein grafts consistently show wall thickening and stiffness under arterial pressures and flow conditions.

In conclusion, venous hypertensive models are typically small animal models (i.e. rat and rabbits) which produce a static 2-fold increases in venous pressure. The present data is inconclusive as to whether or not the venous wall thickens due to venous hypertension. On the other hand, venous grafts consistently show wall thickening and stiffness due to the increases in intraluminal pressure, blood flow and cyclic loading due to pulsatility that are associated with being introduced into the arterial system. Vein graft studies are not translational to CVI. Veins affected by CVI, may experience pulsatile flow and increases in pressure but not to the degree of the artery. There exists a need for a venous hypertensive large animal model induced by chronic venous reflux.

1.3 Biomechanics

The major question this thesis sets out to answer is: how does the venous wall of the common iliac vein remodel in response to chronic venous hypertension due to chronic venous reflux. The objective of biomechanics is to develop, adapt, and apply the laws, theories, and principles of mechanics to answer questions of clinical importance like this one [28]. Vascular biomechanics is a specialty area which seeks to increase the understanding of the physiology and pathophysiology of the vasculature. Many of the basic concepts of vascular biomechanics are well established. Advancements in the field are due to investigation of the responses of specific vascular tissue to applied loads. The biomechanical properties of vascular tissue and their underlying microstructure can aid in the understanding of the basic function of the vessel as well as the development of disease pathology [40]. Compared to the arterial tissue, the investigation of biomechanical properties of the venous tissue is limited. Venous wall biomechanics is decades behind the understanding of the arterial wall [15]. However,

there has been a growing interest in the venous physiology and pathophysiology due to increasing incidences of venous disease [37].

A substantial part of vein function is dependent on its mechanical characteristics and reaction to mechanical forces. Continuum mechanics-based constitutive relations are used to describe a materials behavior under specific conditions of interest. The key concepts of continuum mechanics are stress (force/area), strain (a dimensional change/reference dimension), and rate of deformation; while conservation of mass, momentum, and energy are the governing physical laws [41].

Kinematics is an important component in the understanding of continuum mechanics. Kinematics is the study of motion. In vascular biomechanics, motion refers to how the position of a point within a particular configuration of a tissue has changed relative to its position in a reference configuration. Simplistically, motion refers to the displacement experienced by a particular point on the tissue [28]. The three configurations of interest are: the zero stress condition, the no load condition, and the loaded condition. Figure 1.3 shows the cross-sectional representation for all three configurations. The no load condition (state 1) is the configuration in which there is zero transmural pressure and zero axial load [42]. The zero stress condition (state 0) is the configuration produced when a vessel in the no load condition cut is radially. When veins are cut and examined histologically, there is defect in the circumferential integrity of the vessel wall, usually referred to as opening of the ring. This result is due to residual stress. Residual stress is the stress that exists in the wall in the absence of applied loads [43–47]. This opening of the ring (open angle) implies that in the no load condition, the inner wall is in compression while the outer wall is in tension [48]. Thus, the zero stress condition is the configuration in which there is zero transmural pressure, zero axial load, and zero residual stress [49]. Lastly, the loaded condition (states 2, 3 ... N) is the condition in which the vessel is under transmural pressure and axial force. Each time either the pressure and/or axial stretch is changed a new loaded condition is produced [42].

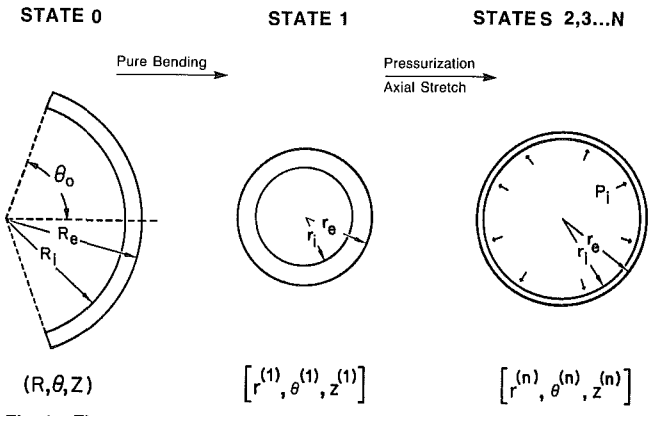

Fig. 1.3. Cross-sectional representation of an artery at the zero stress (state 0), no load (state 1), and subsequent loaded conditions under transmural pressure and axial force (states 2,3 ... N) [42].

Material properties of the tissue can be mathematically described, using continuum mechanics-based constitutive relations derived from the stress and strains, at all the loaded conditions, determined experimentally using either the zero stress condition or the no load condition as the reference configuration [41]. In order for a continuum mechanics-based constitutive relation to be derived, the general characteristics of the material based on its composition and observed behavior must be defined [28]. Biomechanical studies assume the vein to be a viscoelastic, preconditioned, nonlinear, homogeneous, anisotropic, and a incompressible cylinder that is capable of large distensibilities [50–52]. For a vein, which acts as a cylindrical tube, there are three directions of interest: circumferential, longitudinal, and radial. Figure 1.4, depicts the cylindrical coordinate system used for the vein.

Viscoelastic behavior is exhibited by materials that contain both solid and fluid constituents [53]. Characteristics of viscoelastic behavior include creep, stress relaxation, and hysteresis [54]. Creep is a time-dependent deformation under the action of a constant load. Stress relaxation is a time-dependent decrease in load for a constant deformation. Experimentally, hysteresis is when the loading and unloading curves do not coincide. Conceptually, hysteresis occurs when not all strain-energy stored in

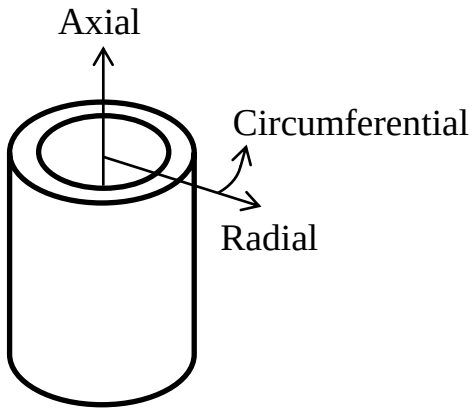

Fig. 1.4. Schematic of the cylindrical coordinate system used.

the material is recoverable [28]. In the absence of smooth muscle tone, blood vessels exhibit hysteresis under cyclic loading, stress relaxation under constant extension, and creep under constant loads. The presence of all three qualifies vascular tissue as a viscoelastic material. Fung proposed that viscoelastic vascular behavior could be regarded as non-linearly pseudoelastic in many problems involving preconditioning [55]. Preconditioning is the process in which repeated cycles of loading yield a steady state response [56, 57]. Blood vessels exhibit a nearly repeatable response to cyclic loading once they have been preconditioned [55, 58].

A pseudoelastic tissue is not elastic but, under periodic loading and unloading, it responds like an elastic material. An elastic material response implies that: (1) the loading and unloading paths coincide, (2) the material responds is instantaneous and time-independent to an applied load, and (3) the material returns to its former unloaded configuration upon the removal of external loads [28]. If venous tissue was truly elastic, the loading and unloading curves would match, but even with preconditioning this does not occur [59]. Thus, the assumption of pseudoelaticity treats the loading and unloading curves as two separate entities [55]. Although, the venous tissue does respond instantaneously to an applied load in a time-independent manner and the material returns to its former unloaded configuration upon the removal of ex-

ternal loads. Pseudoelastisity is merely an appropriate description of the relationship that exists between stress and strain, it is not an intrinsic property of the tissue [60].

Non-linear behavior implies that the relationship between stress and strain in vascular tissue does not form a straight line [61]. Instead, a exponential relationship between the stress and strain in typically observed [62]. Data by Weizsacker et al. validates this exponential type relationship by showing that veins are compliant at lower pressures while rather inextensible at higher pressures (>30 mmHg) [63].

In a homogeneous material, the response to an applied load is independent of the position within the tissue. The distribution of the main constituents within the total wall greatly varies layer to layer. Thus, from the inner diameter to the outer diameter the distribution of the five constituents of the wall varies, making the wall of a healthy vessel heterogeneous [10, 64]. However, in the biomechanical analysis, all stress and strains are calculated with respect to the zero stress condition. Since the same vessel and position within the specimen are being compared, the venous tissue may be referred to as a homogeneous material [28].

Anisotropy implies that the response of the material to an applied load is dependent of the direction of loading. The load displacement curves are dependent of the fiber orientation when a material is anisotropic [65]. Due to the alignment of the collagen and elastin fibers, the circumferential and axial stress-strain relationships will be different [66, 67].

Lastly, incompressibility suggests that a tissue preserves its volume regardless of the loading conditions. The physical motivation behind this assumption is that water is nearly incompressible. Since vascular tissues are mainly composed of water, their walls may be assumed to be nearly incompressible as well, but in actuality no material remains incompressible under all loads and all conditions. However, the analytical and experimental simplification afforded by the assumption of incompressibility is believed to outweigh errors that arise due to the condition not being an exact representative of physics [28, 68].

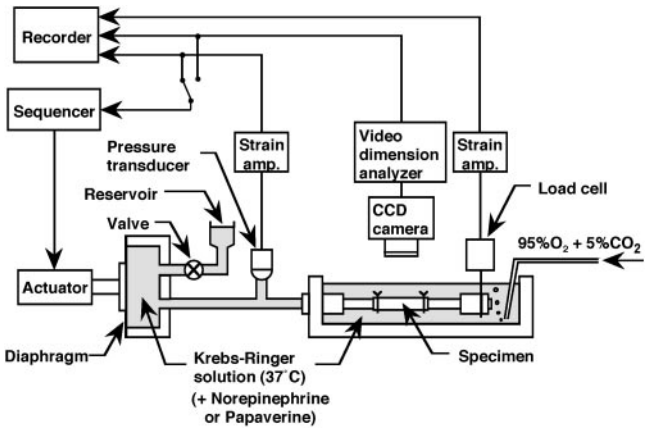

Fig. 1.5. Illustrates the conventional inflation-extension experimental setup used by Hayashi et al. [31].

Assuming a vessel segment is an incompressible cylinder, the mechanical properties in the axial and circumferential directions are obtained using the inflation-extension test [10, 31, 40, 63, 69–72]. In the conventional inflation-extension protocol, the specimen is mounted in a fluid filled bath. Figure 1.5, shows the experimental set up used by Hayashi et al. [31]. Once the vessel is mounted, it is extended to various lengths and inflated by internal pressure. The force, exact pressure, and outer diameter are measured at each length and internal pressure. The outer diameter of the vessel is determined with either a laser beam micrometer [70,72] or a video dimension analyzer combined with a camera [31,63,69,71]. Incompressibility assumes that the product of all the directional (axial, circumferential, and radial) changes, at a given load, will be equal to one ($\lambda_z \lambda_\theta \lambda_r = 1$) [71]. This allows the investigators to calculate the loaded state inner diameter of the vessel based off the directly measured outer diameter and reference thickness. The inner diameter at the loaded state is a critical factor in determining the Green strain and Cauchy stress in the circumferential direction as well as the axial Cauchy stress. Thus, directly measuring the inner diameter would allow for the stress and strain to be calculated without assuming any dimensions. No method exists in which both the inner and outer diameters are measured during the inflation-extension test. Experimentally measuring the inner and outer diameters

at the loaded state would give essential information on how vessels distribute their volume at different loads as well as eliminate the need to assume incompressibility. This is essential since assumptions should be based primarily on the physics, not mathematical convenience.

1.4 Objectives

The primary objective of this thesis is to quantify the passive biomechanical response and structural remodeling of venous tissue subjected to chronic venous hypertension due to reflux. A novel reflux induced venous hypertensive large animal model is introduced as well as a novel method which eliminates the need for the incompressibility assumption. The scope of this thesis may be split into three specific aims:

Specific Aim 1: Develop a reflux induced venous hypertensive large animal model. Hypothesis: If the tricuspid valve is disturbed, then venous reflux will be created which onsets venous hypertension.

Specific Aim 2: Define the passive biomechanical properties using intravascular ultrasound (IVUS) in conjunction with the conventional inflation-extension test. This aim is achieved by four sub aims. Hypothesis: If venous wall is subjected to venous hypertension and chronic venous reflux, then the passive mechanical properties of the venous tissue will change such that the tissue will become stiffer.

Specific Aim 2.1: Validate or invalidate the use of IVUS in inflation test with axial stretch. Hypothesis: If the volume change of the arterial wall is directly calculated, then it will be equal to 1. If the volume change of the arterial wall is not equal to 1, then IVUS is not validated.

Specific Aim 2.2: Define the mechanical properties of the healthy canine Common Iliac vein without the incompressibility assumption. Hypothesis: If IVUS is validated in the artery, then IVUS may be used in the inflation-extension test for veins. If the veins are incompressible, then the volume change of the venous wall will be equal to

1. If the volume change of the venous wall is not equal to 1, then the vein wall is not as incompressible as the artery and the incompressibility assumption should not be used to define the mechanical properties.

Specific Aim 2.3: Define and compare the mechanical properties of the diseased canine common iliac vein to control canine common iliac vein. Hypothesis: If venous wall is subjected to venous hypertension due to chronic venous reflux, then the circumferential Green stain will be lower than the control vessel at the same Kirchhoff stress. At the same axial stretch ratio the diseased circumferential stress-strain curve will shift up and to the left which signifies that the vein wall stiffened in the circumferential direction.

Specific Aim 2.4: Define the constitutive equations for the control and diseased veins. Hypothesis: If a strain energy function is calculated and the material constants are determined, then the material constants will decrease as axial stretch increase and the material constants will be higher in the control vessel than the diseased vessel.

Specific Aim 3: Define if and how the main biomechanical constituents of the venous wall remodel due to venous reflux and hypertension. Hypothesis: If the venous wall is subjected to venous hypertension and chronic venous reflux, then the overall thickness of the wall will increase in addition to the composition of collagen and elastin in the wall changing.

2. MATERIALS AND METHODS

2.1 Animal Model

To develop a large-animal model of chronic venous reflux and hypertension, 9 mongrel dogs underwent disruption of the chordae tendineae with a chordae tendineae cutting device pulled retrograde across the tricuspid valve from the right ventricle to the right atrium. Nine male mongrel dogs with body weight of 34.1 $\pm$ 2.3 kg (mean $\pm$ standard deviation (SD)) were sedated with acepromazine (0.02 mL) and torbugesic (0.7 mL) administered subcutaneously. General anesthesia was maintained with 2 to 3% isoflurane and oxygen. Heparin (1.5-3 mL) was administered every half an hour to prevent coagulation. The flow conditions in the common iliac vein was assessed using duplex ultrasound in the conscious, standing position and the sedated, supine position at five time points: 4 week post-injury, 5 weeks post-injury, 6 weeks post-injury, 7 weeks post-injury and 8 weeks post-injury. Eight weeks after the disruption of the chordae tendineae the animal was euthanized with a bolus of saturated KCl (potassium chloride). All experimental procedures were performed in accordance with national and local ethical guidelines including the Institute of Laboratory Animal Research guidelines, Public Health Service policy, the Animal Welfare Act, and were approved by Institutional Animal Care and Use Committee at Indiana University Purdue University, Indianapolis. A timeline of the animal model protocol is shown in Figure 2.1.

2.1.1 Creation of Venous Reflux

A baseline pulse wave velocity (PWV) tracing for the common iliac vein was recorded in the conscious, standing position and the sedated, supine position, us-

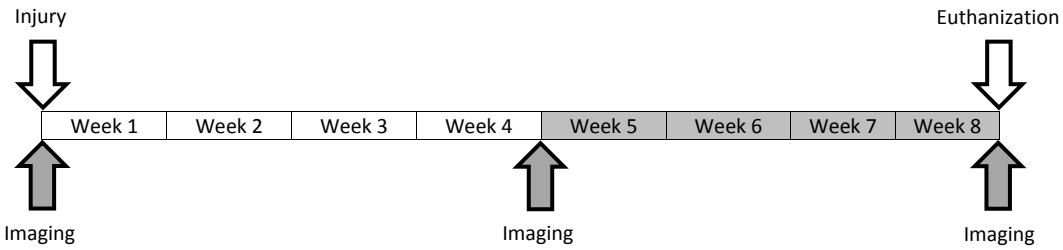

Fig. 2.1. Timeline of the animal model protocol

ing duplex ultrasound (L15-7io Transducer, iE33 Echocardiography System, Phillips; Andover, MA). Once baseline duplex data was obtained, the dogs neck was prepared and draped in a sterile fashion. Access was gained with micro-puncture through the jugular vein. A VISIONS PV .018 Intravascular Ultrasound (IVUS) imaging catheter (86700, Volcano; San Diego, CA) in conjunction with the s5i imaging system (S5iVC01, Volcano) was advanced from the jugular vein down to the common iliac vein. The maximum diameter, minimum diameter, and cross sectional area was obtained for both of the common iliac veins. An external compressional force was applied to the abdominal cavity. An IVUS loop was recorded during compression for both common iliac veins. A frame was selected in which the vein was at maximum distension. The maximum diameter, minimum diameter, and cross sectional area (CSA) was then obtained for the selected frame.

Hemodynamic measurements were made throughout the injury procedure using two fluid-filled pressure transducers (TSD104A, BIOPAC Systems; Coleta, CA). One pressure transducer was attached to the jugular sheath and allowed for jugular venous pressure (JVP) to be obtained; while the other pressure transducer was attached to the catheter and allowed for pressure at the tip of the catheter to be measured. The pressure transducer associated with the catheter allowed for femoral venous pressures (FVP), right atrial pressures (RAP), and right ventricle pressures (RVP) to be obtained.

Once the baseline pressure data (FVP, JVP, RAP, and RVP) was obtained, a chordae tendineae cutting device (Cook Medical; Bloomington, IN) was introduced into the right ventricle. The cutting device was pulled back from the right ventricle to the right atrium in a rotational sweeping motion. The purpose of this was to cut the chordae tendineae which attach the tricuspid valve to the papillary muscles. During this process the electrocardiogram (ECG) was carefully monitored. After each sweep, the RAP and RVP were checked to see if any noticeable changes had occurred. When a mean RAP that was double the baseline RAP was achieved, the cutting device was retracted and the maximum JVP was observed. When a doubling of both the mean RAP and the maximum JVP was observed, then the injury was considered complete. Once the final JVP, RAP, and RVP were taken, the access site was sutured and pressure was applied to the site until hemostasis was achieved. PWV tracing for the common iliac vein was recorded in the sedated, supine position using duplex ultrasound to assess the post-injury flow conditions. Duplex ultrasound was used to ensure that venous reflux was present in the lower extremity veins due to the disrupted tricuspid valve. The animal was then recovered.

2.1.2 Duplex Ultrasound Imaging

The flow conditions in the left and right common iliac veins were assessed using duplex ultrasound. The flow conditions were assessed in both the conscious, standing position and the sedated, supine position at five time points: 4 week post-injury, 5 weeks post-injury, 6 weeks post-injury, 7 weeks post-injury and 8 weeks post-injury. The dogs were again sedated and anesthetized as described above in order to obtain the duplex ultrasound data needed in the sedated, supine position.

2.1.3 Reflux Fraction

The PWV tracings at each time point were used to calculate the reflux fraction in the vessel of interest: the common iliac vein. An image analyzer (ImageJ, National

Institutes of Health) was used to determine the reflux fraction. Compared to the control non-injured velocity measurements (Figure 2.2A) venous reflux was noted immediately after the tricuspid valve was disrupted (Figure 2.2B). Reflux is indicated by the negative velocities (as seen in the PWV tracing post-injury) as opposed to the baseline tracing (which does not exhibit reflux) where none of the velocity waveform crosses zero. The reflux fraction is calculated by integrating the velocity (area under the curve). The integral of velocity is displacement. The portion of the waveform which is above the x-axis represents the displacement of forward flow while the portion of the waveform which is below the x-axis represents the displacement of reverse flow. The reflux fraction can be expressed as the displacement of reverse flow over the displacement of forward flow. Four waveforms were measured per PWV tracing and the four subsequent reflux fractions were averaged.

2.1.4 Euthanization

Eight weeks after injury, the animal was euthanized with a bolus of saturated KCl. Immediately following euthanization, the lower extremity venous system was exposed and the chest was opened. The heart and desired tissue was harvested. Tissue samples from the right atrial myocardium, popliteal veins, and common femoral veins were collected. Three samples were collected for each tissue and fixed using different methods. The three methods of fixation used were liquid nitrogen, 10% formalin, and phosphate buffered formalin. The common iliac vein was harvested, discussed below, for biomechanical testing and morphological evaluation.

2.2 Tissue Harvesting

2.2.1 Disease Canine Common Iliac Vein

The common iliac vein of nine reflux-induced hypertensive mongrel dogs, 34.4 $\pm$ 2.0 kg (mean $\pm$ SD), were used to perform biomechanical experiments and histological

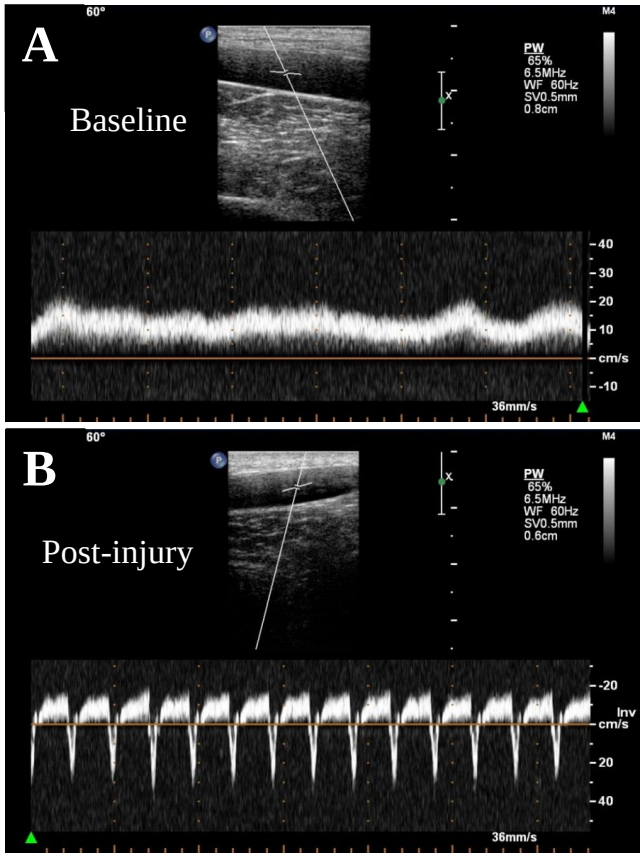

Fig. 2.2. Pulse wave velocity tracings obtained from duplex ultrasound in one dog. A) Baseline common iliac venous flow prior to the creation of injury. B) Immediately after the creation of injury the common iliac venous flow shows notable pulsatility and reflux.

examinations. A suture was placed at the proximal end of the common iliac vein as close to the bifurcation from the inferior vena cava as possible. The suture was tied in a manner in which the knot was placed on the anterior surface of the vessel. Another suture was placed six to eight centimeters distal from the first. Once both ends of the vein were tied off, all visible branches were ligated and the in situ length was measured and recorded. The common iliac vein was then excised, rinsed in room temperature saline, and the ex vivo length was recorded. A two centimeter portion of the proximal end of the vessel was fixed in 10% formalin for histological examinations. Vein segments were fixed in formalin for at least 24 hours prior to any

histological examinations being performed. The remaining segment (∼4-6 cm) was stored in normal saline at 4°C until biomechanical testing. All biomechanical tests were performed within 24 hours of tissue harvest. Prior to biomechanical testing, the adventitia was carefully cleaned under a stereomicroscope (SMZ660, Nikon; Melville, NY). Special care was taken to leave intact adventitia and to not overstretch or mechanically traumatize the vessel.

2.2.2 Control Canine Common Iliac Vein

The common iliac vein of nine control mongrel dogs of either sex weight 24.8 ±2.5 kg (mean ± SD) were used. The animals had been used for other unrelated physiological experiments, performed in accordance with national and local ethical guidelines including the Institute of Laboratory Animal Research guidelines, Public Health Service policy, the Animal Welfare Act, and were approved by Institutional Animal Care and Use Committee at Indiana University Purdue University, Indianapolis. Following sacrifice, the common iliac vein was exposed. The common iliac vein was excised and prepared for biomechanical testing and histological examination in the same fashion as the diseased canine common iliac vein described above.

2.2.3 Control Swine Common Iliac Artery

The common iliac artery of six control domestic swine of either sex weighting 61.8 ±19.0 kg (mean ± SD) were used. The animals had been used for other unrelated physiological experiments, performed in accordance with national and local ethical guidelines including the Institute of Laboratory Animal Research guidelines, Public Health Service policy, the Animal Welfare Act, and were approved by Institutional Animal Care and Use Committee at Indiana University Purdue University, Indianapolis. Following sacrifice, the common iliac artery was exposed. A suture was placed at the proximal end of the common iliac artery as close to the bifurcation for the aorta as possible. The suture was tied in a manner in which the knot was placed on

the anterior surface of the vessel. Another suture was placed six to eight centimeters distal from the first. Once both ends of the artery were tied off, all visible branches were ligated and the in situ length was measured and recorded. Vessel segment were stored in normal saline at 4°C until biomechanical testing. All biomechanical tests were performed within 24 hours of tissue harvest. Prior to biomechanical testing under a stereomicroscope the adventitia was cautiously cleaned, taking care to leave intact adventitia and to not overstretch or mechanically traumatize the vessel.

2.3 Inflation-Extension Test

The experimental setup, shown in Figure 2.3, was used for the inflation-extension bi-axial testing on both veins and arteries. Each tubular specimen was mounted in the bath filled with 3 mM EGTA (ethylene glycol tetraacetic acid) solution kept at room temperature. The 3 mM EGTA solution was prepared by dissolving 1.14 grams of EGTA (34596, Simga-Aldrich; St. Louis, MO) in 1.00 L of normal saline. EGTA is a chelating agent used to restrict Ca^{2+} availability, which allows for the passive vascular wall mechanics to be observed. In the presence of EGTA, the VSMCs are at maximum relaxation. It is assumed, for this study, that the effects of the passive mechanical properties due to VSMCs are negligible and that the passive response results are solely from the mechanical properties of the elastin and collagen [73]. When mounting the vessel onto the inlet and outlet Tygon tubing, special care was taken to not twist or damage the vessel. The specimen was secured to the tubing using 2-0 prolene suture. Special indentations were incorporated into the tubing which allowed for the suture to imbed in and thus allowed the specimen to be securely fixed to the tubing.

A manual syringe pump was used to apply internal pressure to the specimen. The pressure was measured with a fluid-filled pressure transducer (TSD104A, BIOPAC Systems; Coleta, CA), the force was measured with a force transducer (Fort1000, World Precision Instruments; Sarasota, FL), and the inner and outer diameters were determined using an VISIONS PV .018 IVUS imaging catheter (86700, Volcano; San

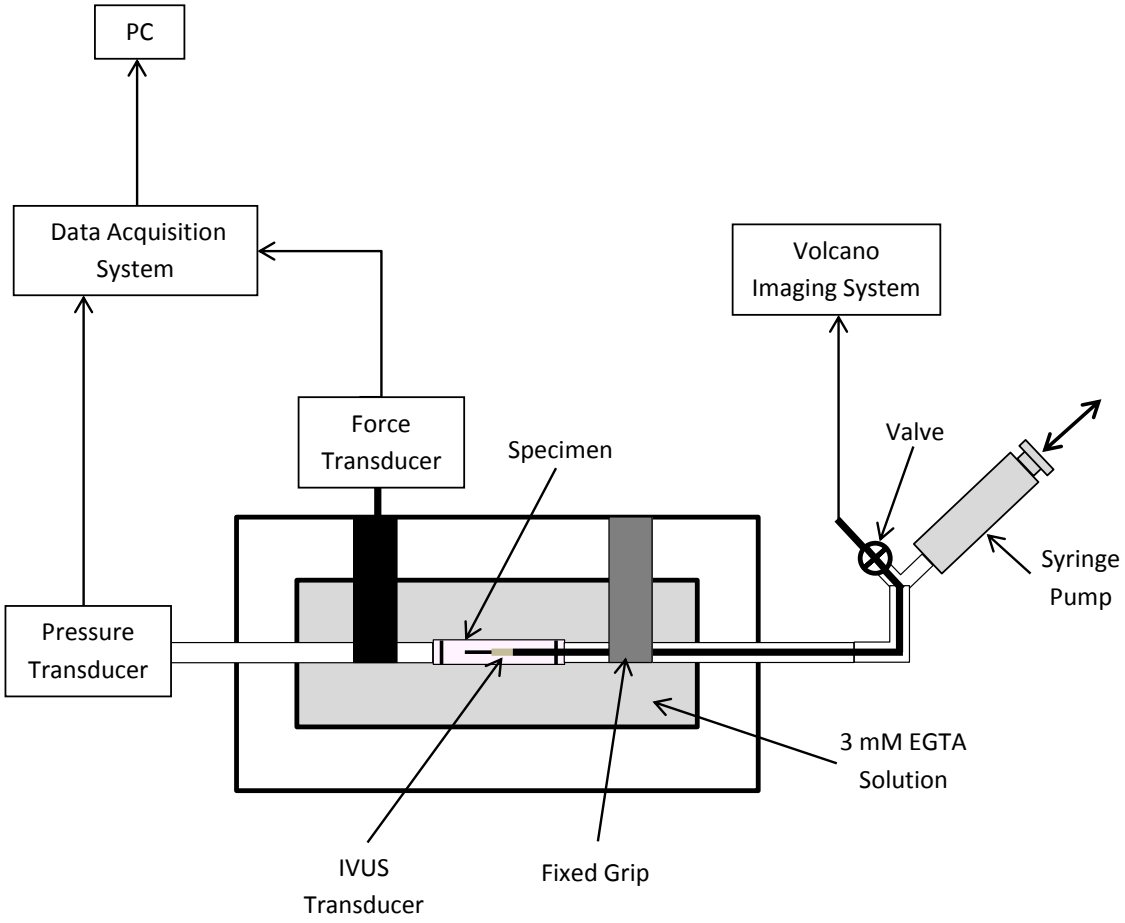

Fig. 2.3. Schematic of the experimental setup

Diego, CA) in conjunction with the s5i imaging system (S5iVC01, Volcano; San Diego, CA).

The pressure and force signals were acquired using a MP150 data acquisition and analysis system (Biopac) and stored in a PC using AcqKnowledge Acquisition and Analysis software (Biopac). Pressure and force signals were amplified using general purpose transducer 1000 gain amplifiers (DA100C, Biopac). The IVUS catheter was set at a center frequency of 20 MHz. The pressure signal was sampled at a frequency of 300 Hz, while the force signal amplifier was sampled at a frequency of 50 kHz.

Once mounted, the diameters and length under no load (no axial stretch and 0 mmHg pressure) were measured. The vessel was then preconditioned at the no axial load state by means of three inflation-deflation loops. The veins were preconditioned using an inflation-deflation loop between the internal pressures of 0 and 60 mmHg, while the arteries were preconditioned using an inflation-deflation loop between the internal pressures of 0 and 120 mmHg. Once the pressure-diameter curve was reproducible, the vessels were perfused by the syringe pump with 3mM EGTA solution at the various perfusion pressures. In veins, static pressure was generated using a stepwise function from 0 to 60 mmHg. The pressure was increased in 5 mmHg step increments from 0 to 20 mmHg and in 10 mmHg step increments from 20 mmHg to 60 mmHg. In the arteries, static pressure was generated using a stepwise function from 0 mmHg to 120 mmHg. The pressures were increased in 10 mmHg step increments from 20 to 60 mmHg and in 20 mmHg step increments from 60 to 120 mmHg. Data was captured at eight specific intraluminal pressures. For the veins, the pressures of interest were 5 mmHg, 10 mmHg, 15 mmHg, 20 mmHg, 30 mmHg, 40 mmHg, 50 mmHg, and 60 mmHg. For the arteries, the pressures of interest were 20 mmHg, 30 mmHg, 40 mmHg, 50 mmHg, 60 mmHg, 80 mmHg, 100 mmHg, and 120 mmHg. At each point of interest, the pressure and force measured by the transducers were recorded as well as a still image was captured with IVUS. Figure 2.4 is an example of the raw data produced during each inflation cycle. This specific run was for the control canine vein extended to its 100% physiologic length.

An axial load was applied to the vessel by extending it to its 80% physiologic length. The physiologic length is determined by the physiologic stretch ratio. The physiologic stretch ratio used the in situ and ex vivo lengths which were recorded at the time the tissue was harvested and is defined as:

$$\lambda_{phys} = \frac{\text{in situ length}}{\text{ex vivo length}} \tag{2.1}$$

Thus, 100% physiologic length is the product of the physiologic stretch ratio and the length measured under no load. Therefore, 80% physiologic length is equivalent

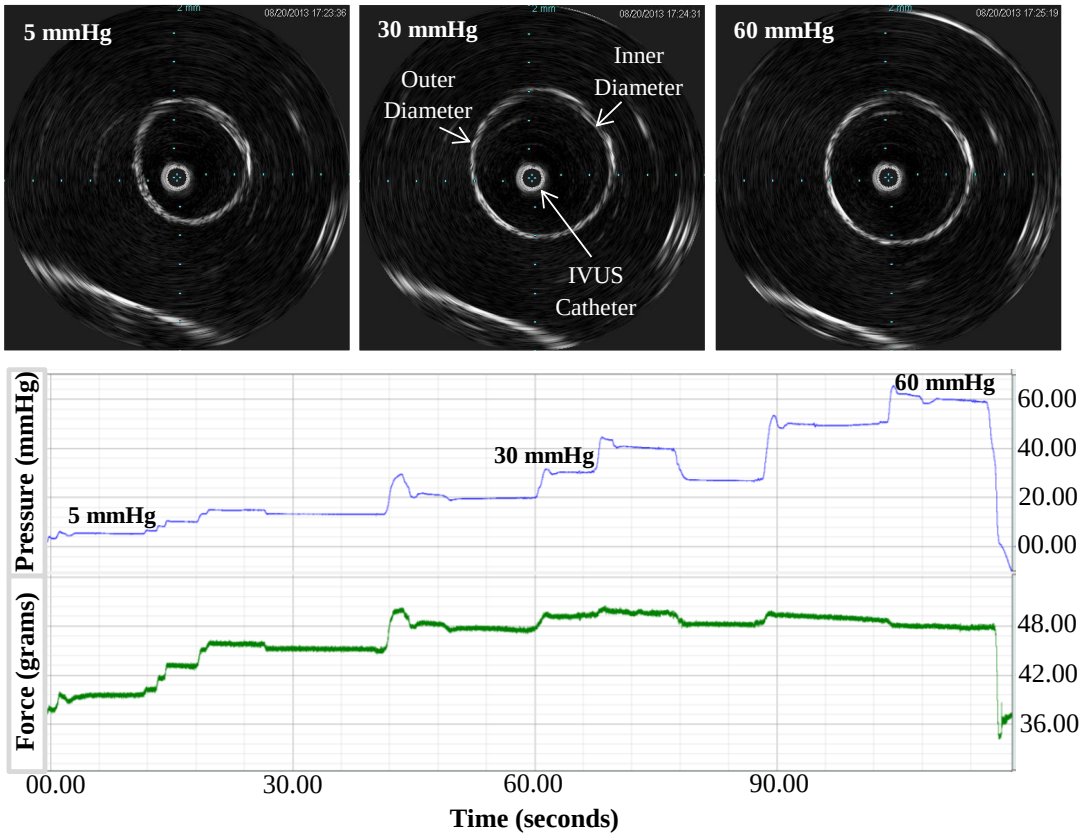

Fig. 2.4. Raw data produced for one inflation cycle at 100% physiologic length extension in control common iliac vein. The three images on the top panel illustrate the IVUS images captured by the Volcano imaging system at 5, 30, and 60 mmHg. The middle panel shows the real time pressure as well as the corresponding axial force (bottom panel) during the inflation cycle.

to 0.80 of the 100% physiologic length. Once the axial load was applied, the vessel was once again preconditioned by means of three inflation-deflation loops. Once preconditioned, the vessel was inflated using the stepwise function mentioned previously. Force, pressure, and IVUS images were obtained at the eight pressures defined above. Once all the data was collected at the 80% physiologic length condition, all the load (both axial and circumferential) was released. This protocol was then repeated for extensions of 90%, 100%, and 110% physiologic length. Every time a new axial load was applied, the specimen was preconditioned.

2.3.1 IVUS versus Digital Camera

In conventional inflation-extension tests, the outer diameter of the specimen was measured using either a laser micrometer or a video dimension analyzer in combination with a digital camera. To determine the agreement between the conventional experimental method (digital camera) and the proposed experimental method (IVUS) the outer diameter of the specimen was measured with both IVUS and the digital camera during the inflation-extension tests. Five specimens, two control canine common iliac vein and three control swine common iliac arteries, were used. Different species and vessels were tested in order to represent all control specimens which were used in the biomechanical testing. A digital camera (PC1742, Canon) was added to the existing experimental set up and placed vertically above the specimen. At each point of interest, the pressure and force were measured by the transducers and were recorded. In addition, two still images were captured concurrently: one using IVUS and one using the digital camera. The outer diameter was calculated for each image using an image analyzer (ImageJ, NIH). The Bland-Altman method was used to measure the agreement between IVUS and the digital camera.

2.4 Zero Stress Reference State

At the end of the inflation-extension test, three 2 mm thick rings were cut at different locations along the vessel. The rings were placed in a bath filled with normal saline, which was kept at room temperature, and its cross-sectional image was captured using WinFast PVR (Leadtex; Tiawan) via a stereoscope (SMZ660, Nikon; Melville, NY) and a CCD camera (STC-630AS, SenTech; Carrollton, TX). The anterior portion of the ring was then cut and another image was captured. The resulting images represent the vessel in the no stress condition (Figure 2.5a) and zero stress condition (Figure 2.5b).

When the excised, intact, unloaded vessel was radially cut the ring opened up. The angle in which the vessel opens up when it is radially cut is called the open

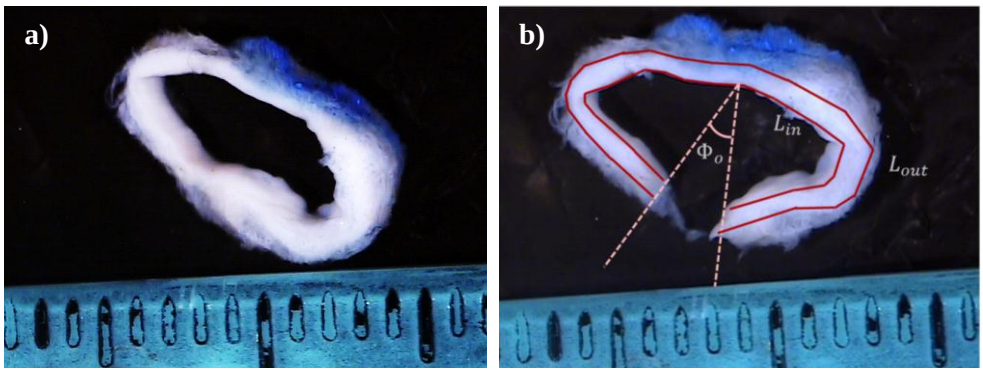

Fig. 2.5. Cross-sectional area of control common iliac vein at a) no stress condition and b) zero stress condition.

angle (Φ_o). The effects of radially cutting a vessel in the no load condition and the resulting open angle can be seen in Figure 2.5. Two other important measurements, in addition to the open angle, were obtained from the zero stress images. They were the inner radius (R_{in}) and outer radius (R_{out}). In order to obtain (R_{in}) and (R_{out}), the inner arc length (L_{in}) and outer arc length (L_{out}) of the cut vessel was measured using an image analyzer (ImageJ). Figure 2.5b shows the L_{in}, L_{out}, and Φ_o of a control common iliac vein. The inner and outer radii are determined using a basic geometric formula. The arc length formula states:

$$L = \frac{n^\circ}{360} \times 2\pi R \tag{2.2}$$

Solving for R produces:

$$R = \frac{L \times 360}{n^\circ \times 2\pi} \tag{2.3}$$

where,

$$n^\circ = 360 - 2\Phi_o \tag{2.4}$$

Therefore,

$$R_{in} = \frac{L_{in} \times 360}{n^{\circ} \times 2\pi} \tag{2.5}$$

$$R_{out} = \frac{L_{out} \times 360}{n^{\circ} \times 2\pi} \tag{2.6}$$

The zero stress condition thickness, T, was calculated using the values obtained for R_{out} and R_{in}. Such that:

$$T = R_{out} - R_{in} \tag{2.7}$$

2.5 Loaded Condition

The loaded condition is due to axial and circumferential load. Thus, the loaded condition is dependent on the pressure and axial extension. The inner and outer radii at the loaded condition were determined from the still images captured by IVUS. Using the ShowCase DICOM Viewer, the still images captured by IVUS were converted to JPEG images. The inner and outer circumferences were then measured using an image analyzer (ImageJ, NIH) and the inner and outer radii were calculated by dividing the corresponding circumference by 2π.

The thickness at the loaded condition is defined as:

$$t = r_{out} - r_{in} \tag{2.8}$$

2.6 Principal Stretch Ratios

The vessel was assumed to be a hollow cylinder and was assigned a cylindrical coordinate system as shown in Figure 2.6a. The deformation was assumed to be cylindrically orthotropic. This means the vessels response to an applied load is unique in all three directions (circumferential, axial and radial). The parameters associated with the loaded condition can be seen in Figure 2.6b, while the parameters associated with the reference zero stress condition can be seen in Figure 2.6c.

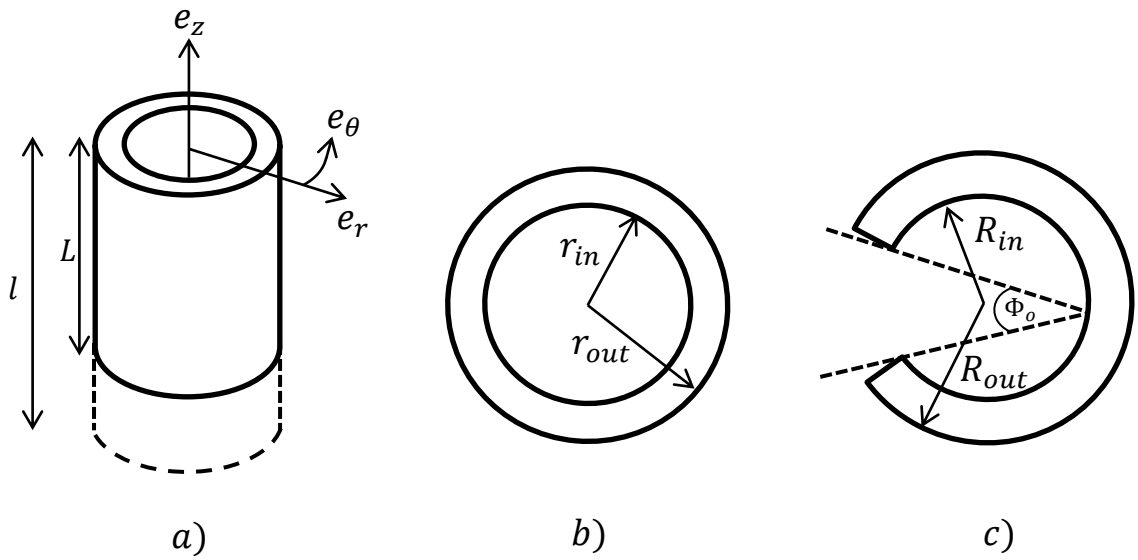

Fig. 2.6. Schematic of a) Isometric view of cylindrical coordinate system, b) loaded condition, and c) zero stress condition

The principal stretch ratios are the primary deformations associated with the radial, circumferential, and axial directions due to loading [74]. They are defined by the following equations with the zero stress condition as the reference condition:

$$\lambda_z = \frac{l}{L} \tag{2.9}$$

The axial length at the loaded condition is l while L is the length at the unloaded condition.

$$\lambda_\theta(r) = \frac{\chi r}{\sqrt{\chi(r^2 - r_{in}^2)\lambda_z + R_{in}^2}} \tag{2.10}$$

$$\chi = \frac{180}{180 - \Phi_o} \tag{2.11}$$

Equation (2.10) shows that the circumferential stretch ratio is dependent on the radial location. The circumferential stretch ratio at the inner radius of the loaded state is defined as:

$$\lambda_\theta(r_{in}) = \frac{\chi r_{in}}{R_{in}} \tag{2.12}$$

And the circumferential stretch ratio at the outer radius of the loaded state is equivalent to:

$$\lambda_\theta(r_{out}) = \frac{\chi r_{out}}{\sqrt{\chi(r_{out}^2 - r_{in}^2)\lambda_z + R_{in}^2}} \tag{2.13}$$

In order to obtain an insight into the general behavior of the vessel wall the average circumferential stretch ratio is used in all further equations. The average circumferential stretch ratio is defined as:

$$\lambda_\theta(r_{average}) = \frac{\lambda_\theta(r_{in}) + \lambda_\theta(r_{out})}{2} \tag{2.14}$$

r_{in} is the inner radius at the loaded condition, r_{out} is the outer radius at the loaded condition, and $r_{average}$ is the mean of the inner radius and the outer radius at the loaded condition.

The radial stretch ratio is defined as:

$$\lambda_r = \frac{\delta r}{\delta R} \tag{2.15}$$

Conventionally, the vessel wall is assumed to be incompressible. If the wall volume does not change due to stress it may be assumed that:

$$\lambda_\theta \lambda_z \lambda_r = 1 \tag{2.16}$$

Solving for λ_r gives,

$$\lambda_r = \frac{1}{\lambda_z \lambda_\theta} \tag{2.17}$$

The radial stretch ratio, equation (2.17), is defined as the differential of the radial direction in terms of the loaded condition over the differential of the radial direction in terms of the zero stress condition. Simply put,

$$\lambda_r = \frac{t}{T} \tag{2.18}$$

Using IVUS, the values of r_{in} and r_{out} were obtained for all the loaded conditions. Equation (2.8) states that the value of t is obtained directly from r_{in} and r_{out}. Additoinally, T is also directly obtained from equation (2.7). Thus, the radial stretch ratio was directly measured using equation (2.18).

2.7 Stress-Strain Relationship

2.7.1 Green Strain

The axial Green strain is defined as:

$$E_{zz} = \frac{(\lambda_z^2 - 1)}{2} \tag{2.19}$$

Since the stretch ratio is the only variable that drives the Green strain, the circumferential Green strain is also dependent of the radial location. However, to obtain an insight to the general behavior of the vessel, the average radius is used to compute the values of stain and stress. Therefore, circumferential green strain is:

$$E_{\theta\theta}(r_{average}) = \frac{(\lambda_\theta(r_{average})^2 - 1)}{2} \tag{2.20}$$

2.7.2 Cauchy Stress and Kirchhoff Stress

The axial Cauchy stress is dependent on the pressure (P), force (F), inner diameter and outer diameter at the loaded condition. Therefore, axial Cauchy stress is:

$$\sigma_z = \frac{F + P\pi r_{in}^2}{\pi(r_{out}^2 - r_{in}^2)} \tag{2.21}$$

The circumferential Cauchy stress in thin-walled veins was determined using Laplaces law [75, 76]. Thus, circumferential Cauchy stress is a function of pressure. It is dependent on the pressure, inner radius, and thickness at a given pressure.

$$\sigma_\theta = \frac{P \times r_{average}(P)}{t(P)} \tag{2.22}$$

The axial Kirchhoff stress is obtained from the Cauchy stress and axial stretch ratio and is defined as:

$$S_z = \frac{\sigma_z}{\lambda_z^2} \tag{2.23}$$

Where the circumferential Kirchhoff Stress is:

$$S_\theta = \frac{\sigma_\theta}{\lambda_\theta^2} \tag{2.24}$$

2.7.3 Mathematical Model

The strain energy function (SEF) represents the stored energy per unit volume of the venous wall. In two dimensional analyses the SEF is a second order polynomial since the radial and all shear components are neglected. A Fung-type SEF was implemented [77]:

$$W = C(e^Q - 1) \tag{2.25}$$

$$Q = \alpha_1 E_{\theta\theta}^2 + \alpha_2 E_{zz}^2 + \alpha_4 E_{\theta\theta} E_{zz} \tag{2.26}$$

The Fung-type SEF is a function of the Green Strains in the axial, E_{zz}, and circumferential, $E_{\theta\theta}$, directions. The specimens material constants are expressed as C, α_1, α_2, and α_4. Where C is a component of stress expressed in kPa and α_1, α_2, and α_4 are non-dimensional. In response to an increase in strain, the number of stretched molecules and the tension force within the stretched molecules will increase. Since blood vessels do not obey Hookes law, the increase in strain is not equal to the increase in stretched molecules and the resulting tension force. However, they are directly proportional. Thus, α_1 is the proportionality constant in the circumferential direction, α_2 is the proportionality constant in the axial direction, and α_4 refers to the cross talk between the circumferential and axial direction. Lastly, the constant C is a scaling factor [60].

The material constants are obtained using the experimental Green Stains, $E_{\theta\theta}$ and E_{zz}, and the theoretical Kirchhoff stresses:

$$S^*_{\theta\theta} = C(\alpha_1 E^2_{\theta\theta} + \alpha_4 E^2_{zz})e^Q \tag{2.27}$$

$$S^*_{zz} = C(\alpha_4 E^2_{\theta\theta} + \alpha_2 E^2_{zz})e^Q \tag{2.28}$$

The material constants for each vessel at each longitudinal stretch ratio were calculated mathematically. Arbitrary values were entered as the values for C, α_1, α_2, and α_4. The arbitrary values and the known the Green Strains, $E_{\theta\theta}$ and E_{zz}, at each longitudinal stretch ratio and pressure were inputted into equation (2.27) and equation (2.28) [78]. This produced values for $S^*_{\theta\theta}$ and S^*_{zz}. The theoretical Kirchhoff stresses, $S^*_{\theta\theta}$ and S^*_{zz}, were then compared with the experimental Kirchhoff stresses, $S_{\theta\theta}$ and S_{zz}. The sum of squares of the difference between the theoretical and experimental Kirchhoff stresses was calculated using the SUMXMY2 function in Excel (Microsoft). The objective was to get the sum of squares of the difference between the theoretical and experimental Kirchhoff stresses as close to zero as possible by changing the material constants. This was done by using the data solver function in Excel. The data solver function determined the best values for the material constants to create the minimum discrepancy between the experimental and theoretical Kirchhoff stresses. To determine how good a fit the constitutive equations were the correlation coefficient was calculated for both the axial and circumferential data. The non-linear correlation coefficient is defined as:

$$r = \sqrt{1 - \frac{SSE}{SST}} \tag{2.29}$$

With:

$$SSE = \sum (y_i - y_{f_i})^2 \tag{2.30}$$

$$SST = \sum (y_i - \overline{y})^2 \tag{2.31}$$

Where y is the experimental Kirchhoff stress, y_f is the theoretical Kirchhoff stress, $\bar{y}$ is the mean experimental Kirchhoff stress for the inflation cycle and $i = 1 - 8$ since there were eight corresponding pressures per stretch ratio.

2.8 Histological Evaluation

2.8.1 Histological Preparation of Common Iliac Vein

As mentioned above, a two centimeter long segment of each common iliac was fixed in formalin. Each of those segments was cut into two 1 cm long rings. One segment was used for basic morphology, while the other one was used for multiphoton microscopy (MPM). For basic morphology, the vessel rings were rinsed three times with a buffer solution, processed by dehydration in increasing concentrations of alcohol (70, 80, 95, and 100%), and embedded in glycol methacrylate (JB-4 solution, Electron Microscopy Sciences). The embedded segments were cut into 3-μm-thick sections using a conventional microtome (model HM 340E; Microm), mounted on glass slides, and stained with toluidine blue. The histological sections were photographed using Spot Insight Color digital camera (Diagnostic Instruments) attached to a histological microscope (Eclipse E600; Nikon), and wall thickness measurements were made from these images using ImageJ (National Institutes of Health).

For MPM, the vessel rings were frozen in Neg-50 gel using liquid nitrogen (Richard-Allan Scientific Neg -50; Thermo Scientific). The frozen segments were cut into 40-μm-thick sections using a conventional cryostat set at -25°C (model CM1850; Leica), mounted on glass slides, surrounded by 25 μL of glycerol-phosphate buffer solution (PBS) solution (70% Glycerol 30% PBS), and encased with a glass cover slip. Prepared slides were kept in 4°C refrigerator until MPM was performed.

2.8.2 Multiphoton Microscopy

MPM is the combination of two primary types of nonlinear interaction between ultrafast laser light and biological tissues: two-photon excited fluorescence (TPEF) and second-harmonic generation (SHG). TPEF is used to depict elastin that contains endogenous fluorophores, while SHG signal originates from collagen type I that contains molecular noncentrosymemtric structures [79]. MPM images of both control and diseases venous tissue were obtained using a Multiphoton Laser Scanning Microscope (FV1000 MPE, Olympus). The microscope is an inverted system and multiphoton fluorescence excitation provided by fully automated Spectra-physics MaiTai DeepSee laser (excitation wavelength from 710 nm to 990 nm). The average excitation power at the sample was 1.4 W with an excitation wavelength of 860 nm. The dichroic mirror RDM690 was used to separate SHG (430 nm) and TPEF ($\sim$520 nm) signals from the excitation beam and then directed toward photomultiplier-tube (PMT) detectors. A 20X W .95NA water immersion objective (XLUMPLFL; Olympus America) was used for all specimens, and each acquired image covered an area of 634.7 x 634.7 μm^2. The step size between slices was typically set at 2 μm, and the number of slices for one site was $\sim$12. The scan time for an entire Z stack was $<<$1 min.

Four essential images were captured using MPM (represented in Figure 2.7): Light microscopy image, TPEF image, SHG image, and SHG/TPEF image. In order to quantify the relative amount of each venous wall component, the SHG and TPEF images were individually imported into an image analyzer (ImageJ, NIH), and made into binary images. The venous wall area was then selected and the percent area was determined. The resulting percentage represented the proportion of collagen or elastin to the total area selected. The percent areas were calculated for collagen and elastin in both control and diseased venous tissue using the percent area function in ImageJ.

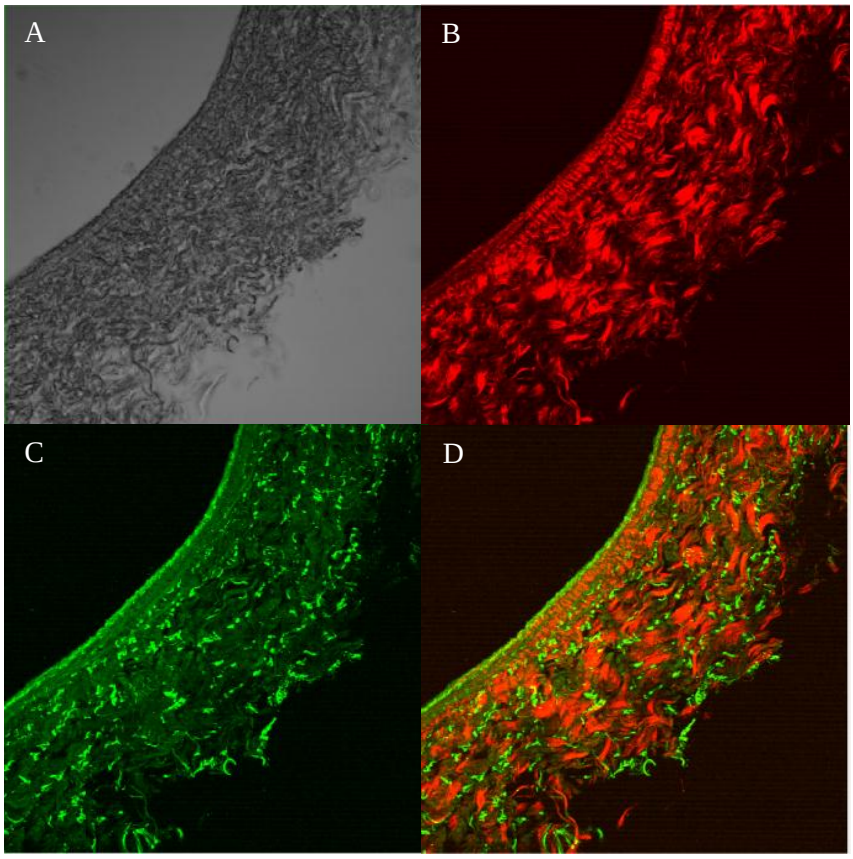

Fig. 2.7. Representation of the four images obtained with multiphoton microscopy (MPM) for the control common iliac vein: A) Light microscopy image, B) SHG image depicting collagen content within venous wall, C) TPEF image depicting the elastin content within the venous wall, and D) Merged SHG/TPEG image depicting the distribution of collagen and elastin within the venous wall.

2.9 Statistical Analysis

All data was expressed as mean ± standard error (SE) unless otherwise specified. The biomechanical parameters were compared using ANOVA. A students t-test was used to detect possible differences between the control and diseased tissue. A paired t-test was used to detect possible differences in venous pressure and reflux fraction at different time points in the reflux induced hypertensive dogs. Significance was defined as $p < 0.05$.

3. RESULTS

3.1 Reflux Induced Hypertensive Canine Model

3.1.1 Venous Reflux

Following the creation of venous reflux through the disruption of the chordae tendineae of the right side of the heart the tricuspid valve became partially dislocated. Figure 3.1 shows the mean pressure in the right atrium and right ventricular prior to and after the chordae tendineae were disrupted and the tricuspid valve was partially dislocated. Prior to disruption (labeled as baseline) the mean RAP was 3.19 ± 0.37

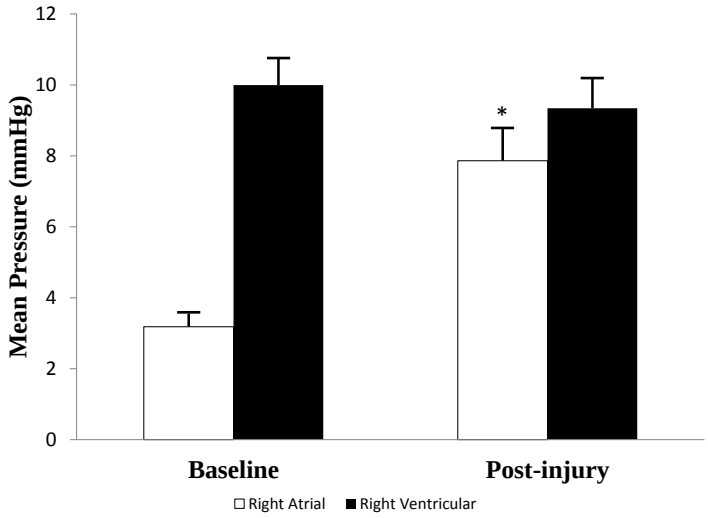

Fig. 3.1. Mean pressure in right atrium and ventricle prior to (baseline) and after (post-injury) chordae tendineae were disrupted. Figure shows grouped average for n = 9 dogs. Mean ± Standard Error (SE). $*$ $p < 0.05$ vs. Baseline right atrial pressure.

mmHg and the mean RVP was 10.00 ± 0.75 mmHg. After injury (post-injury), the mean RAP significantly increased to 7.86 ± 0.89 mmHg, while the mean RVP was unchanged.

The mean RAP after injury was 2.41 times greater than prior to injury. Figure 3.2 confirms a significant 3.5-fold increase in peak JVP due to the disruption of the chordae tendineae. The maximum JVP post-injury, 4 weeks post-injury (4 weeks), and 8 weeks post-injury prior to euthanization (8 weeks) were all significantly higher than the baseline maximum JVP. However, after injury there was no significant increase in maximum JVP as time progressed (post-injury vs. 4 weeks post-injury: $p = 0.21$, 4 weeks post-injury vs. 8 weeks post-injury: $p = 0.31$, and post-injury vs. 8 weeks post-injury: $p = 0.98$).

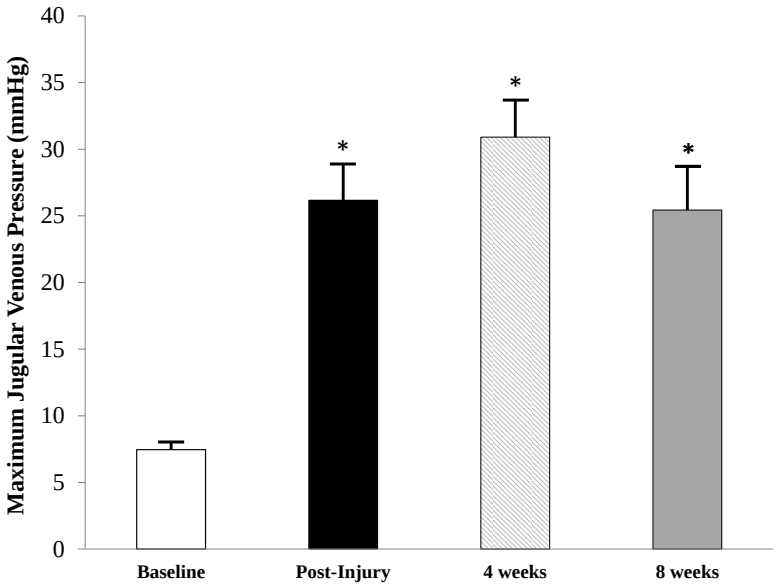

Fig. 3.2. Maximum pressure in the jugular vein before (baseline), after chordae tendineae are disrupted (post-injury), 4 weeks post-injury (4 weeks), and 8 weeks after injury prior to euthanization (8 weeks). Figure shows grouped average for $n = 9$ dogs. Mean ± SE. $* p < 0.05$ vs. Baseline.

Prior to injury, the dogs had a mean reflux fraction of 0%. Figure 3.3 shows that mean reflux fractions present in the common iliac vein obtained from the PWV tracings after injury, 4 weeks post-injury, and 8 weeks post-injury. Post-injury, a reflux fraction of 23.12 $\pm$ 4.22 % was observed in the common iliac vein. After the initial creation of venous reflux, there was no significant increase in venous reflux observed up to the time of euthanization (post-injury vs. 4 weeks: $p = 0.74$, 4 weeks vs. 8 weeks: $p = 0.94$, and post-injury vs. 8 weeks: $p = 0.52$).

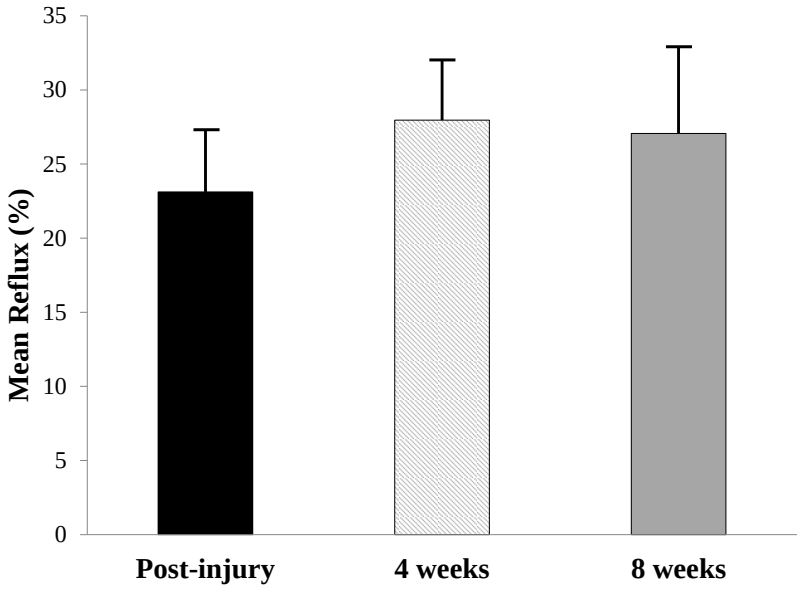

Fig. 3.3. The mean reflux fraction in the common iliac vein after chordae tendineae are disrupted (post-injury), 4 weeks after injury (4 weeks), and prior to euthanization (8 weeks). Baseline (not shown) reflux fraction was 0%. Figure shows grouped average for $n = 7$ dogs. Mean $\pm$ SE. $* p < 0.05$ vs. post-injury.

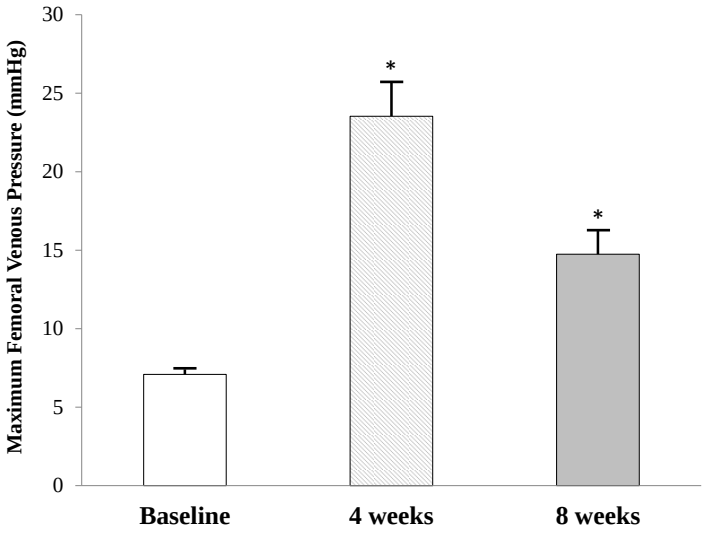

Fig. 3.4. Maximum pressure in the common femoral vein before the chordae tendineae are disrupted (baseline), four weeks after chordae tendineae are disrupted (4 weeks), and prior to euthanization (8 weeks). Figure shows grouped average for n = 9 dogs. Mean ± SE. $*$ $p < 0.05$ vs. Baseline.

3.1.2 Venous Hypertension

Figure 3.4 illustrates the maximum femoral venous pressure (FVP) observed before the chordae tendineae were disrupted (baseline), 4 weeks after injury (4 weeks), and just prior to euthanization (8 weeks). The baseline maximum FVP prior to injury was 7.09 ± 0.31 mmHg. At four weeks post-injury (4 weeks), the maximum FVP observed was 23.04 ± 2.07 mmHg which was a significant increase from baseline maximum FVP ($p < 0.05$). At eight weeks post-injury (8 weeks) a decrease in maximum FVP compared to the pressure observed at 4 weeks was observed, but was found to not be significant (15.25 ± 1.46 mmHg, $p = 0.059$).

Figure 3.5 displays the maximum in vivo inner diameter of the common iliac vein measured with IVUS prior to injury (baseline) and four weeks post-injury (4 weeks).

Effective inner diameters were determined using the CSA obtained with IVUS and equation (3.1).

$$d = \sqrt{\frac{4CSA}{\pi}} \tag{3.1}$$

The effective inner diameter prior to injury was 10.14 ± 0.36 mm, while the effective inner diameter after four weeks of venous reflux was 10.07 ± 0.26 mm. There was no significant difference found between the baseline effective inner diameter and the effective inner diameter after four weeks of venous reflux (p = 0.81).

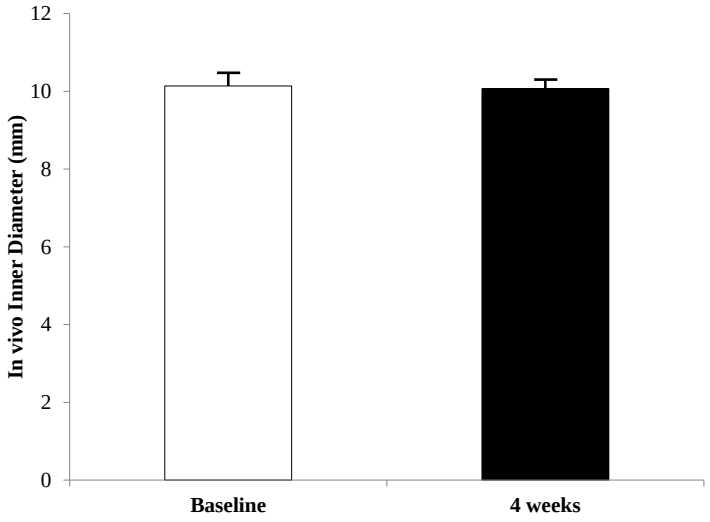

Fig. 3.5. In vivo effective diameter of common iliac vein prior to injury (baseline) and four weeks post-injury (4 weeks). Figure shows grouped average for n = 8 dogs. Mean ± SE. ∗ $p < 0.05$ vs. corresponding baseline diameter.

3.2 Biomechanical Properties

3.2.1 Zero Stress Condition and Physiologic Stretch Ratio

The open angle of the diseased common iliac vein, 74.9 ± 8.6°, was significantly higher than the open angle of the control common iliac vein, 44.9 ± 4.9° (p = 0.007). The inner diameter (R_{in}) and outer diameter (R_{out}) at the zero stress condition of the diseased common iliac vein were significantly larger than the control common iliac vein. The inner diameter (R_{in}) and outer diameter (R_{out}) at the zero stress condition of the diseased common iliac vein were 4.19 ± 0.21 mm and 4.86 ± 0.20 mm. The inner diameter (R_{in}) and outer diameter (R_{out}) at the zero stress condition of the control common iliac vein were 3.25 ± 0.15 mm and 3.71 ± 0.26 mm. The physiologic stretch ratios of the control and diseased common iliac veins were not significantly different (p = 0.56). The physiologic stretch ratio of the diseased common iliac vein was 1.62 ± 0.02, while the physiologic stretch ratio of the control common iliac vein was 1.64 ± 0.03.

3.2.2 Accuracy of IVUS

The agreement between the conventional experimental method (digital camera) and the proposed experimental method (IVUS) for measuring the outer diameter was tested in five vessels. Outer diameter measurements were obtained with the digital camera and IVUS at 48 data points per animal (n = 240). Figure 3.6A shows the relationship between the IVUS measurement and the digital camera measurement. The relationship is described by $y = 1.05x + 0.06$ with an R^2 value of 0.96. The y-intercept indicates that IVUS overestimated the outer diameter by 6.46 %. Figure 3.6B is the Bland-Altman analysis. The Bland-Altman shows the difference and average values of the outer diameters measured by IVUS and the digital camera. The mean difference between the two methods was 0.46 mm with a standard deviation of

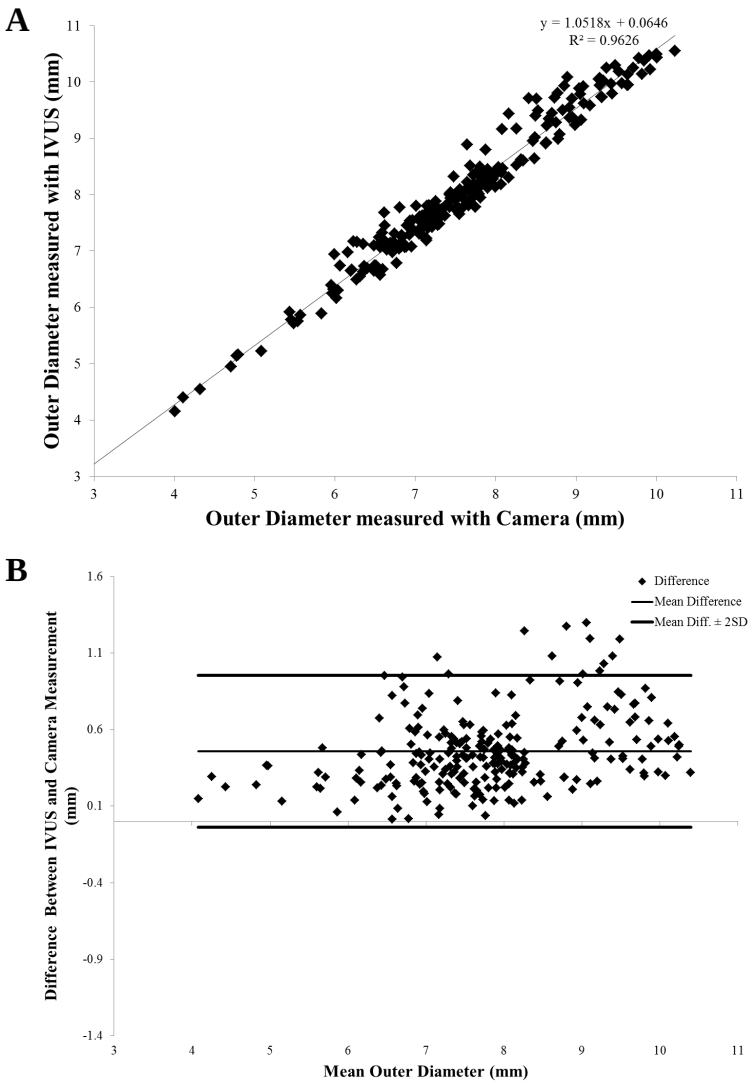

Fig. 3.6. Accuracy of IVUS in measuring the outer diameter of the vessel. A: The identity relationship between the IVUS measurement and the digital camera measurement, with the solid black line as the identity line. B: Bland-Altman analysis. SD, Standard deviation. Figure shows grouped average for n = 240 (48 images per vessel for 5 vessels).

0.25 mm. Of the 240 images compared, there were 11 data points greater than 2 SD away from the mean and hence, were removed from analysis.

3.2.3 Incompressibility

Incompressibility assumes that the volume of the vessels wall does not change. The product of the three directional stretch ratios ($\lambda_\theta\lambda_z\lambda_r$) indicates the change in volume. If a vessel is incompressible, then the change in volume is equal to one. The radial stretch ratio (λ_r), the circumferential stretch ratio (λ_θ), and the axial stretch ratio (λ_z) were experimentally obtained for six control swine common iliac arteries, six control canine common iliac veins, and six diseased canine common iliac veins. Since, both arteries and veins were studied, the loaded condition was used to normalize the data. The 5 mmHg loaded condition was used as the reference configuration. Ideally the 0 mmHg condition would have been used as the reference condition, but that data point was not available for all vessels [42]. The product of the three stretch ratios was determined at 100% physiologic axial length. Figure 3.7 shows the change in wall volume of arteries, control veins, and diseased veins. The bold solid horizontal line represents the incompressibility assumption which assumes that the change in volume is equivalent to one. A 1-sample t-test was performed with a hypothesized mean of 1. There was significance between the experimental mean of both the veins and the hypothesized mean, but there was no significance found between the experimental mean of the artery and the hypothesized mean of 1 ($p = 0.11$). The change in volume for arteries was 0.97 ± 0.02. All experimental results produced ($\lambda_\theta\lambda_z\lambda_r$) values that are less than one. Additionally, there was a significant increase in the change in volume between control (0.64 ± 0.04) and diseased (0.76 ± 0.04) veins.

3.2.4 Pressure-Diameter Relation

The pressure-inner diameter curves for all five axial loads in both control and diseased common iliac veins are shown in Figure 3.8. Figure 3.8A shows the change in inner diameter over pressure for control veins, while Figure 3.8B shows the change in inner diameter over pressure for diseased veins. The pressure-inner diameter curves were non-linear. In both tissues and at all axial loads, the vessel was more distensible

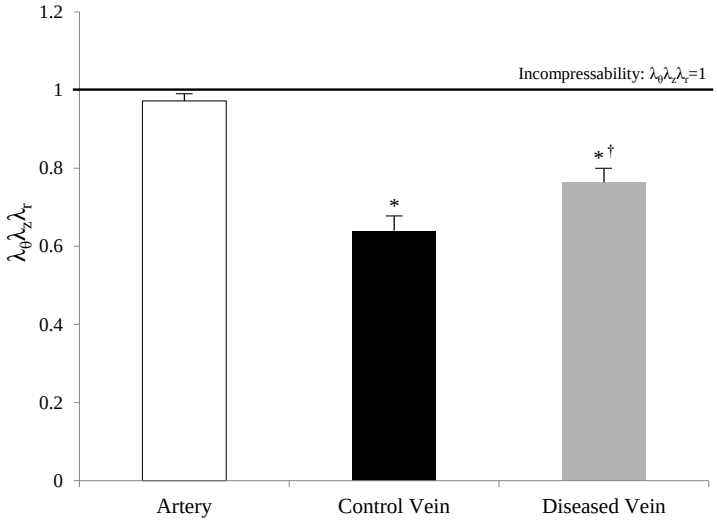

Fig. 3.7. The product of the three directional stretch ratios (change in volume) for control arteries, control veins and diseased veins at 100% physiologic length. The 5 mmHg loaded condition was used as the reference state. Figures shows grouped average for n = 6 dogs. Mean ± SE. ∗ $p < 0.05$ vs. hypothesized mean of 1. † $p < 0.05$ vs. control vein

at lower pressures. Between 0 mmHg and 30 mmHg, small changes in pressure resulted in significant changes in inner diameter. After 30 mmHg the inner diameter begins to plateau and large changes in pressure resulted in minor changes in inner diameter.

Additionally, the axial load significantly affected inner diameter at lower pressures (0-30 mmHg). After 30 mmHg the axial load did not significantly affect the inner diameters. Thus, at lower pressures and at lower stretch ratios the vessel started off at a higher inner diameter. As the stretch ratio increased the inner diameter was smaller at a given lower pressure. The control and diseased veins acted similarly and showed similar non-linear trends. However, in the diseased vessel, the difference between inner diameters at axial stretch ratios larger than 90% is much greater, particularly

at 110% physiologic length where the pressure-inner diameter curve was more linear and did not plateau until ∼50 mmHg.

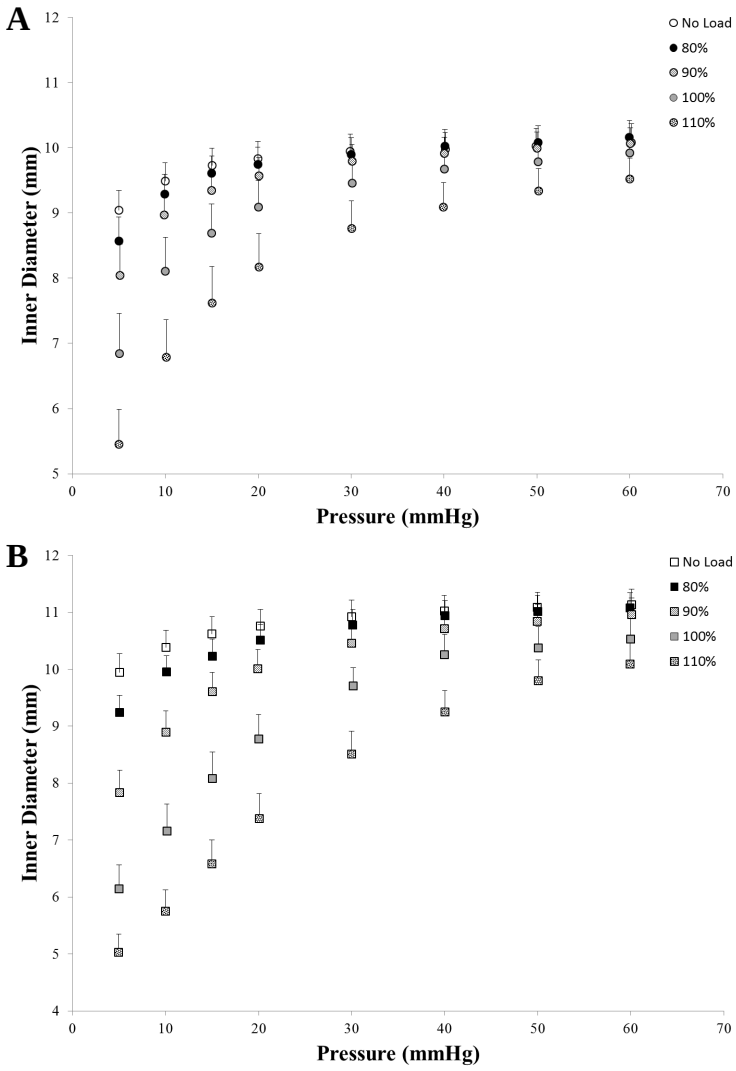

Fig. 3.8. Change inner diameter over pressure of the common iliac veins for the five axial loading conditions. A: Pressure-Inner diameter curves for control canine common iliac veins. B: Pressure-Inner diameter curves for diseased canine common iliac veins. Circles = Control tissue and Squares = Diseased tissue. Figures shows grouped average for n = 9 dogs. Mean ± SE.

Figure 3.9 displays the inner diameter, outer diameter, and thickness versus pressure for control and diseased common iliac veins stretched to 100% physiologic length. Control tissue is represented as circles while diseased tissue is represented as squares. The black symbols represent outer diameter, the no fill symbols represent the inner diameter, and the shaded symbols represent thickness. As pressure increases the inner diameter and outer diameter increased non-linearly, while the thickness decreases non-linearly as pressure increased. The inner and outer diameters of diseased and control veins were not significantly different and did not display a distinct pattern or trend. However, at any given pressure the thickness of the diseased veins was always larger than the control vein. Second order polynomial trend lines were fit to the control and diseased thicknesses. For the control vessel the equation of the trend line

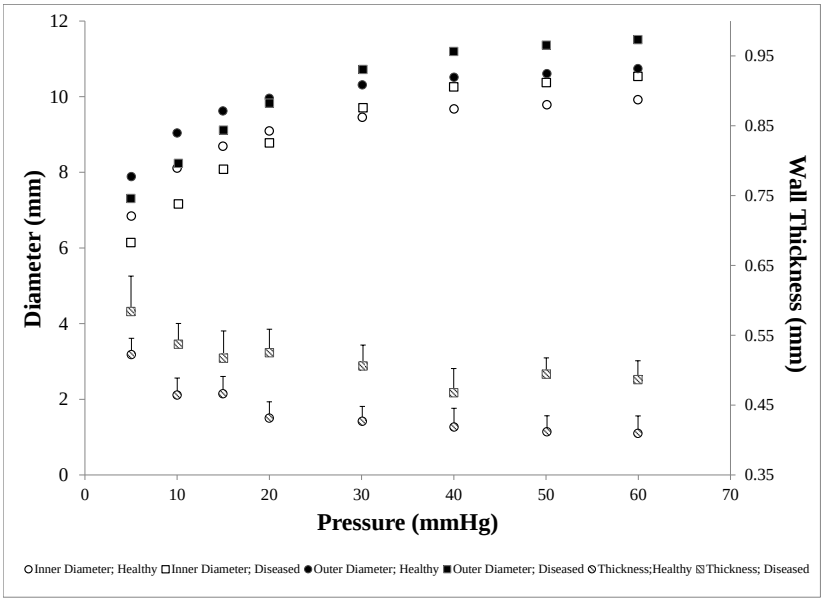

Fig. 3.9. Pressure-diameter curves of the inner and outer diameter of control and diseased common iliac veins at 100% physiologic length. The resulting thickness is plotted against the second axis. Second order polynomial trend lines (solid lines) were fit to the control and diseased thicknesses. Circles = Control tissue and Squares = Diseased tissue. Figures shows grouped average for n = 9 dogs. Mean ± SE.

was $y = .00006x^2 - .053x + .5293$ with a $R^2 = 0.90$, while the equation of the trend line for the diseased vessel was $y = .00005x^2 - .005x + .5942$ with a $R^2 = 0.87$.

3.2.5 Pressure-Axial Kirchhoff Stress Relation

The axial Cauchy stress and Kirchhoff stress were calculated using equations (2.21) and (2.23) with respect to the zero stress condition. Figure 3.10 shows the axial Kirchhoff stress over pressure in both control (Figure 3.10A) and diseased (Figure 3.10B) veins. Both graphs represent the axial Kirchhoff stress-pressure relationship to be linear with a small slope. The horizontal nature of the relation indicates that pressure had only a slight effect on the axial Kirchhoff stress. There was no significant difference between the axial Kirchhoff stressed of control and diseased vessels at the no axial load or 80% physiologic length state. However, for 90% physiologic length axial stretch and above, the diseased vessels exhibited higher axial Kirchhoff stress than the control vessel at a given pressure.

3.2.6 Mechanical Remodeling

The circumferential Cauchy stress was calculated using equation (2.22) with respect to the zero stress condition. Based off the animal model, it was known that the maximum FVP the control common iliac veins experienced was ∼7 mmHg, while the diseased veins experience an average maximum FVP ∼20 mmHg. If all veins respond the same as arteries do to hypertension, then the circumferential Cauchy stress in the diseased vessel at the hypertensive pressure (20 mmHg) would be equal to the circumferential Cauchy stress in the control vessel at the baseline pressure (7 mmHg). Assuming a linear relationship exists between Cauchy stress and pressure, the circumferential Cauchy stress at 7 mmHg was obtained through interpolation (7.86 ± 0.65 kPa) and plotted (Control; 7 mmHg). This value (Control; 7 mmHg) represents what after 8 weeks of chronic reflux the circumferential Cauchy stress should be at 20 mmHg if the vein remodeled like an artery under hypertension and fully compen-

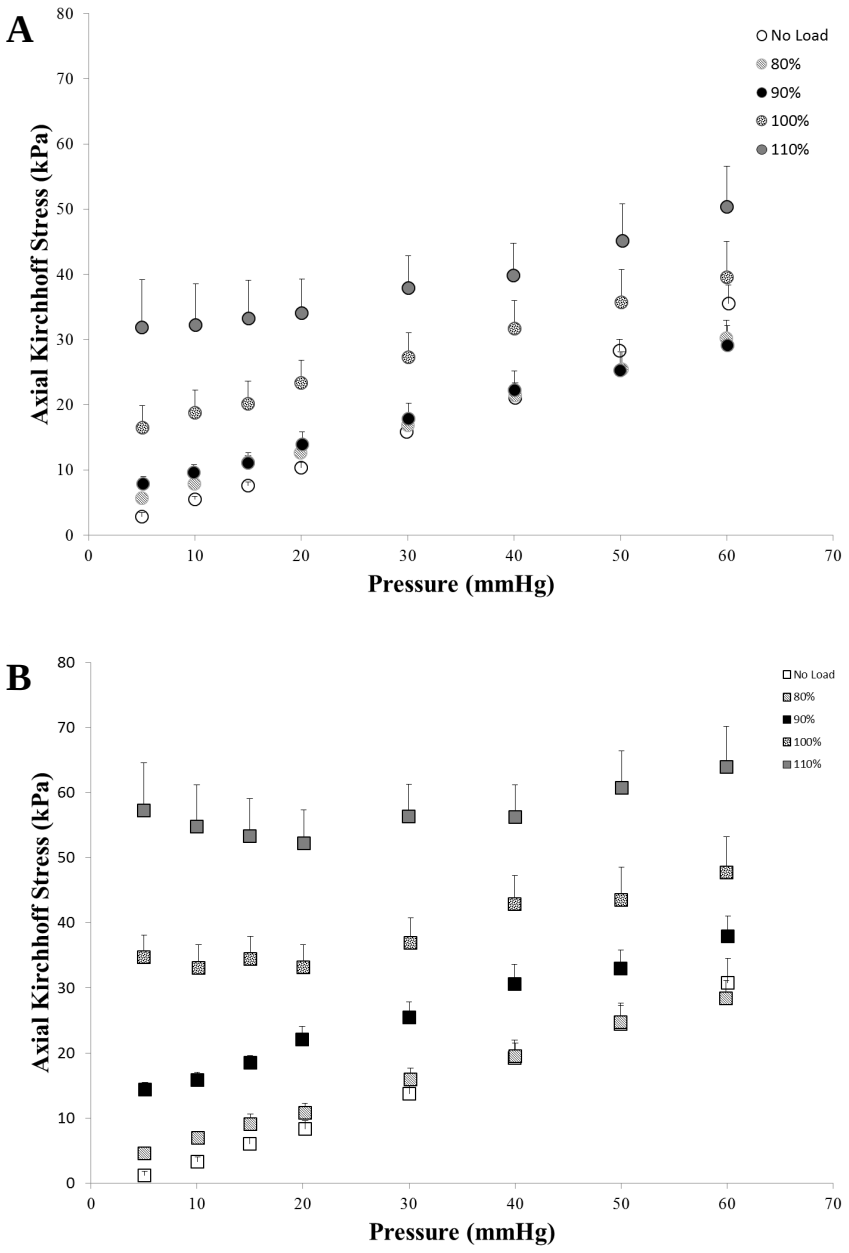

Fig. 3.10. Axial Kirchhoff stress over pressure in canine common iliac veins for the five axial loading conditions. A: Control venous tissue. B: Diseased venous tissue. Circles = Control tissue and Squares = Diseased tissue. Figures shows grouped average for n = 9 dogs. Mean ± SE. Stress calculated with respect to the zero-stress condition.

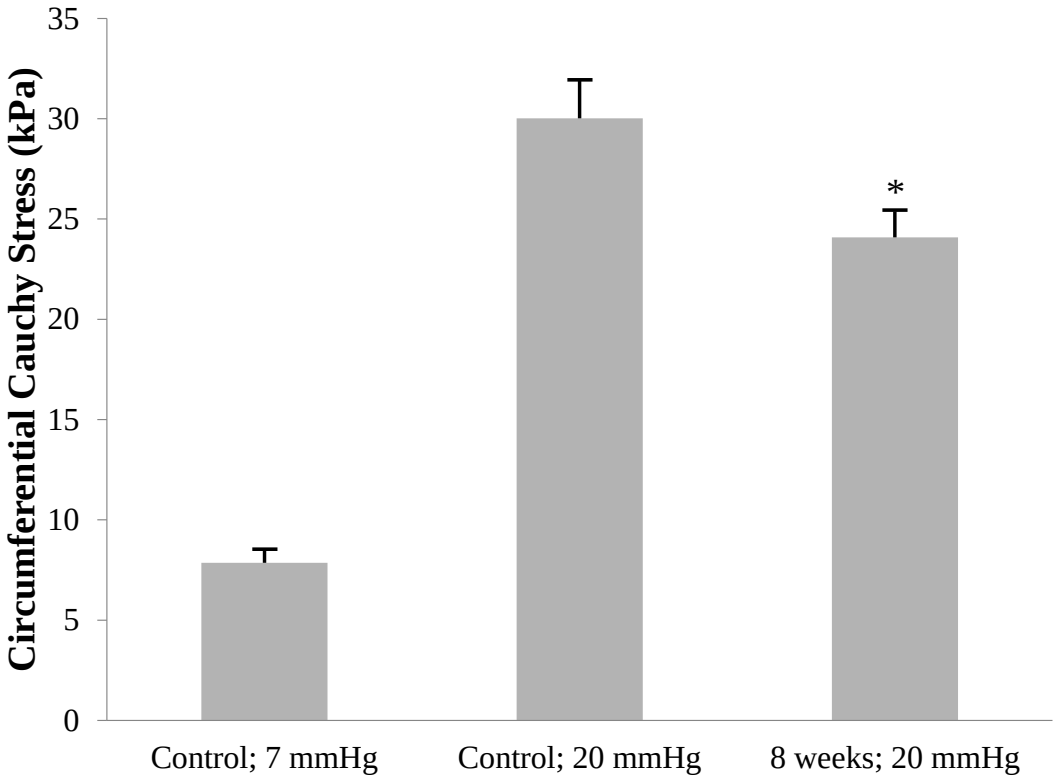

Fig. 3.11. Circumferential Cauchy stress for: the control canine common iliac vein at hypertensive pressure (Control; 20 mmHg), the experimental diseased canine common iliac vein at hypertensive pressure (Diseased; 20 mmHg), and the control canine common iliac vein prior to the increase in venous pressure (Control; 7 mmHg). Figures shows grouped average for n = 9 dogs. Mean ± SE. Stress calculated with respect to the zero-stress condition.

sated for the increase in pressure. Additionally, the circumferential Cauchy stress at 20 mmHg was plotted for both the control (Control; 20 mmHg) and the diseased (Diseased; 20 mmHg) veins. The resulting plot is shown in Figure 3.11. The circumferential Cauchy stress in the diseased vessel at 20 mmHg was significantly lower

than the circumferential Cauchy stress in the control vessel at 20 mmHg (diseased = 24.09 ± 1.29 kPa; control = 30.02 ± 1.92 kPa; p = 0.02). However, eight weeks post-injury the circumferential Cauchy stress of the diseased vessel at 20 mmHg was still significantly higher than the control circumferential Cauchy stress prior to the increase in pressure (p = 0.00).

Based off the experimental Kirchhoff stresses and Green strains, the material constants for each vessel at each axial stretch ratio was calculated mathematically using equation (2.27) and (2.28). All stresses and strains were calculated with respect to the zero stress condition. The material constants for both control and diseased veins at each axial stretch ratio is shown in Figure 3.12. The scaling factor (C) increased as axial stretch ratio increased in both control and diseased vessels. The circumferential proportionality constant (α_1) decreased as the axial stretch ratio increased in both control and diseased vessels. The axial proportionality constant (α_2) did not have a noticeable trend. Lastly, α_4 which is the constant that refers to the cross talk between the circumferential and axial direction, like α_1, decreased as axial stretch ratio increased in both control and diseased tissue. All material constants at all axial stretch ratios were larger for the control veins than the diseased veins. The correlation coefficient for the fit of the experimental data to the mathematical formulation, in the circumferential direction was between 0.95 and 1.00, while the correlation coefficient in the axial direction was between 0.83 and 0.99.

The circumferential Kirchhoff stress and Green strain were calculated using equation (2.24) and (2.20) with respect to the zero stress condition. Figure 3.13A shows the stress-strain curves for the control common iliac vein at the five axial stretch ratios. Figure 3.13B shows the stress-strain curves for the diseased common iliac vein at the five axial stretch ratios. Figure 3.13C shows the stress-strain curves for the control and diseased common iliac vein at the 100% physiologic axial stretch ratio. Using the material constants in Figure 3.12, a Fung-type exponential model was fit to the stress-strain curves. As the axial stretch ratio increases, the curve is shifted up and to the left for both control and diseased vessels. Figure 3.13C illustrates that the

	C (kPa)	α_1	α_2	α_4	Correlation Coef	
		(nondimensional)			S_θθ	S_zz
No Axial Load						
Healthy	8.36E-05	1.32E+01	N/A	1.87E+01	0.95	0.98
Diseased	1.98E-03	1.15E+01	N/A	1.48E+01	0.96	0.97
80% Physiological						
Healthy	5.43E-04	3.04E+00	3.53E+00	1.19E+01	0.98	0.99
Diseased	2.00E-03	3.32E+00	8.40E+00	8.65E+00	0.98	0.99
90% Physiological						
Healthy	7.41E-04	2.76E+00	1.75E+01	2.44E+00	0.99	0.83
Diseased	9.77E-03	2.03E+00	1.36E+01	1.84E+00	0.98	0.86
100% Physiological						
Healthy	8.93E-02	2.02E+00	6.62E+00	2.00E-03	0.97	0.97
Diseased	1.52E+00	9.10E-01	3.35E+00	4.95E-01	0.97	0.97
110% Physiological						
Healthy	5.19E-02	1.95E+00	4.19E+00	3.39E-01	0.99	0.97
Diseased	2.37E+00	6.63E-01	1.91E+00	5.17E-01	1.00	0.92

Fig. 3.12. Material constants for control and diseased canine common iliac veins.

diseased veins stress-strain curve is uniformly shifted up and to the left indicating that at a given strain, the circumferential Krichhoff stress was higher in the diseased vein than the control vein. The Fung-type exponential model fits all data points well at the 110%, 100%, and 90% physiologic axial stretch ratios. However, at lower stresses in the no load and 80% physiologic axial stretch ratios, the Fung-type exponential model does not characterize the experimental data as accurately.

3.3 Microstructural Remodeling

Figure 3.14 displays the histological and merged SHG/TPEG images produced for both a control common iliac vein and a diseased common iliac vein at the no load

condition. Visually comparing Figure 3.14A and Figure 3.14B, there was a noticeable difference in total wall thickness as well as the intimal-medial thickness. Figure 3.15 confirms this visual observation. The total wall thickness significantly increased from 0.44 ± 0.03 mm in control venous tissue to 0.68 ± 0.03 mm in diseased venous tissue. Similarly, the intimal-medial thickness significantly increased from 0.04 ± 4.68E−3 mm in the control venous tissue to 0.11 ± 4.70E−3 mm in the diseased venous tissue. The media makes up 9.07 ± 0.98 % of the total wall thickness in control venous tissue compared to 13.61 ± 0.88 % in the diseased venous tissue. This increase is statistically significant ($p < 0.001$).

MPM was used to depict the elastin using TPEF and the collagen using SHG. The percent area of the total wall area each constituent made up was calculated. Figure 3.16 shows the collagen to elastin ratio of the venous wall for control and diseased common iliac veins. The collagen to elastin ratio significantly increased from 1.38 ± 0.08 in control venous tissue to 2.63 ± 0.29 in diseased venous tissue ($p = 0.008$). Figure 3.17 shows that the both the percent area of both collagen and elastin in the total venous wall decreased in the diseased tissue. However, only the decrease in percent area of elastin had statistical significance. The decrease in collagen content from a percent area of 34.42 ± 2.45 % in control tissue to a percent area of 28.31 ± 2.07 % in diseased tissue was not significant ($p = 0.89$). The significant increase in collagen to elastin ratio was due to the decrease in elastin from 25.57 ± 2.81 % in control tissue to 11.42 ± 1.55 % in diseased tissue ($p = 0.003$).

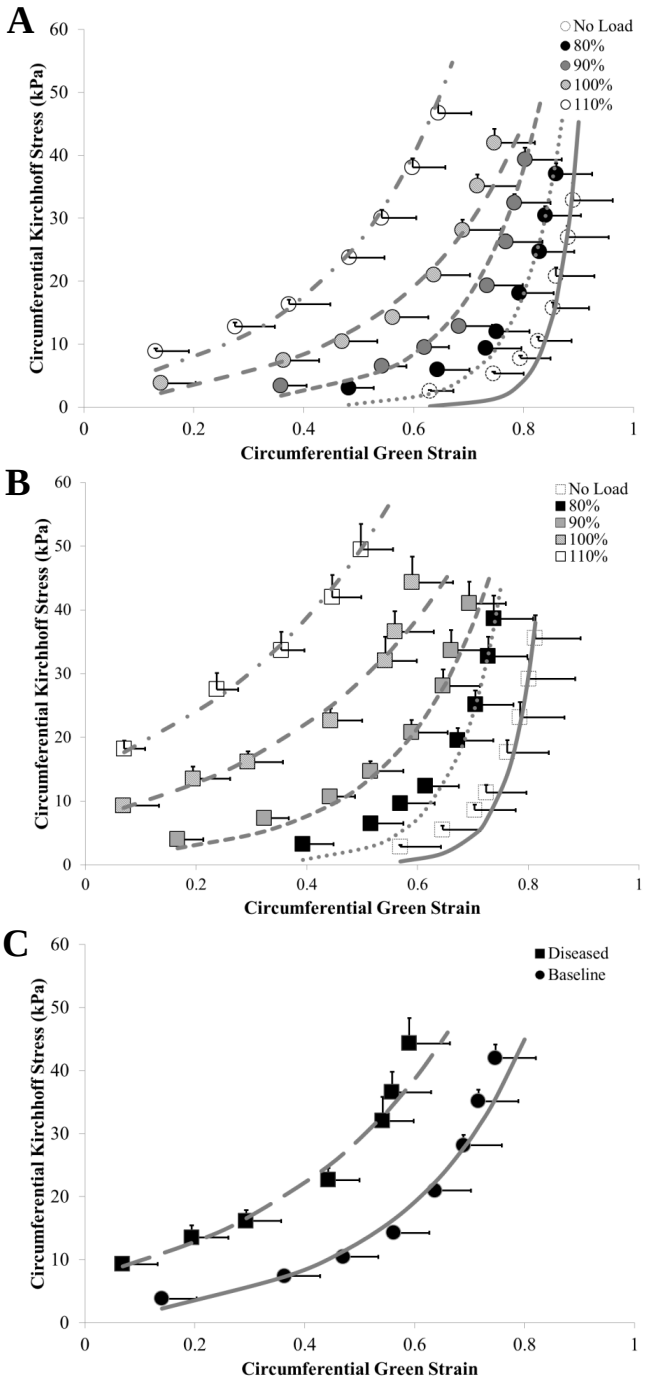

Fig. 3.13. Circumferential Kirchhoff stress-Green strain curves for canine common iliac vein. A: Control vein at the five axial loads. B: Diseased vein at the five axial loads. C: Control vs. Diseased vein at 100% physiologic length. Figures shows grouped average for n = 9 dogs. Mean ± SE. Stress and strain calculated with respect to the zero-stress condition. Each axial load is fit with its corresponding Fung model.

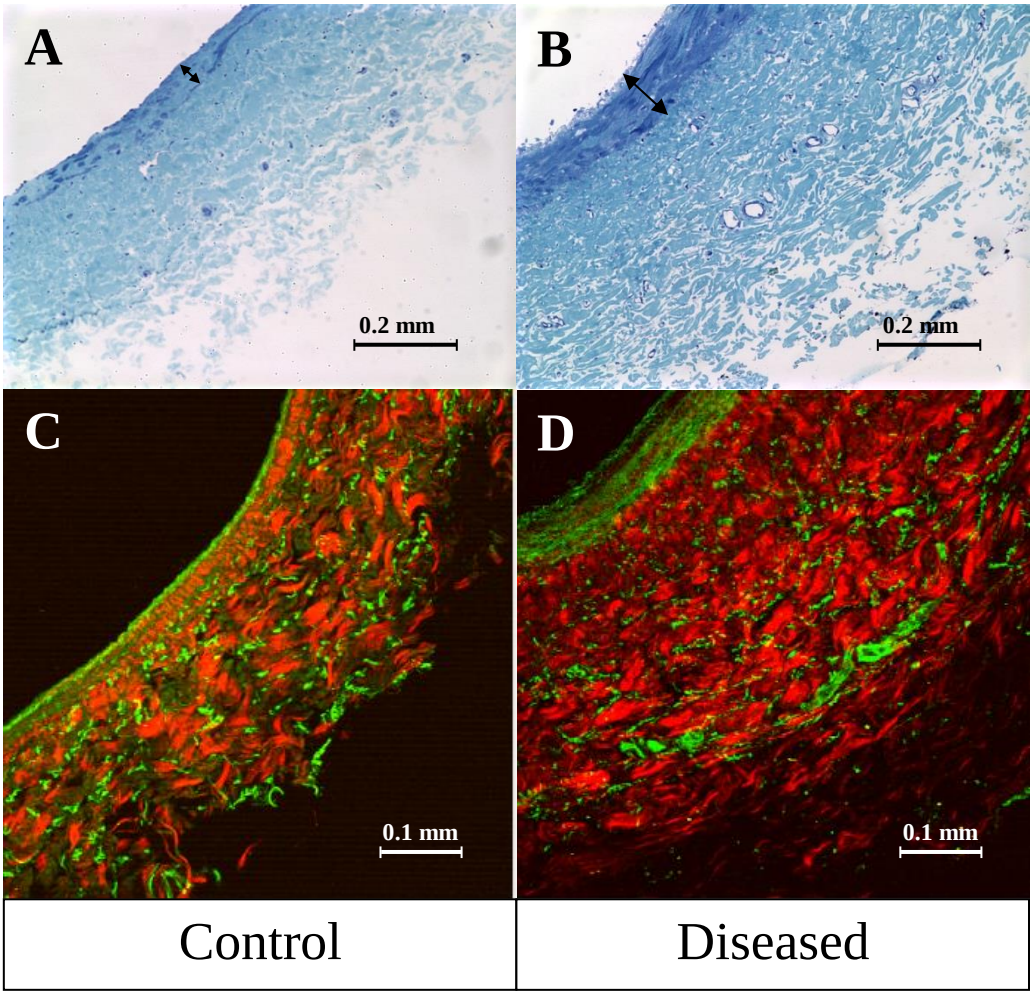

Fig. 3.14. Histological and merged SHG/TPEG images of the common iliac venous wall for control and diseased veins. A: Histological section of a control canine common iliac vein. B: The histological section of a diseased canine common iliac vein. C: Merged SHG/TPEG image of a control canine common iliac vein. D: Merged SHG/TPEG image of a diseased canine common iliac vein. $\longleftrightarrow$ indicates intimal-medial thickness.

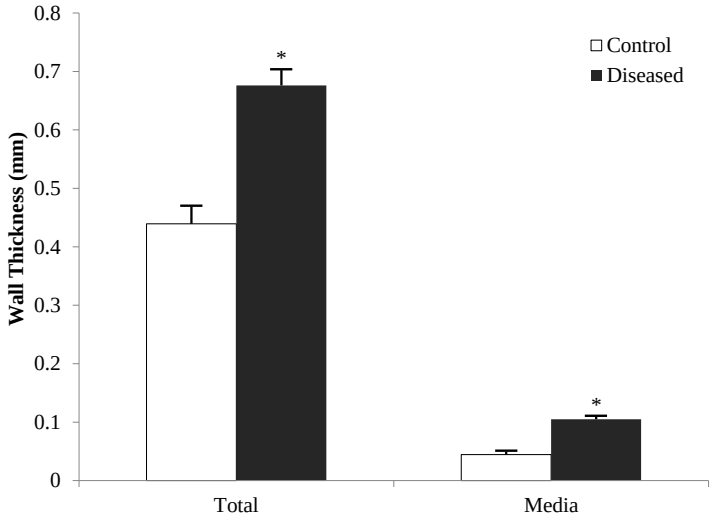

Fig. 3.15. Total wall thickness and intimal-medial thickness at the no load condition in control and diseased canine common iliac veins. Thicknesses measured from histological section images. Figure shows grouped average for n = 6 dogs. Mean ± SE. $*$ $p < 0.05$ vs. control.

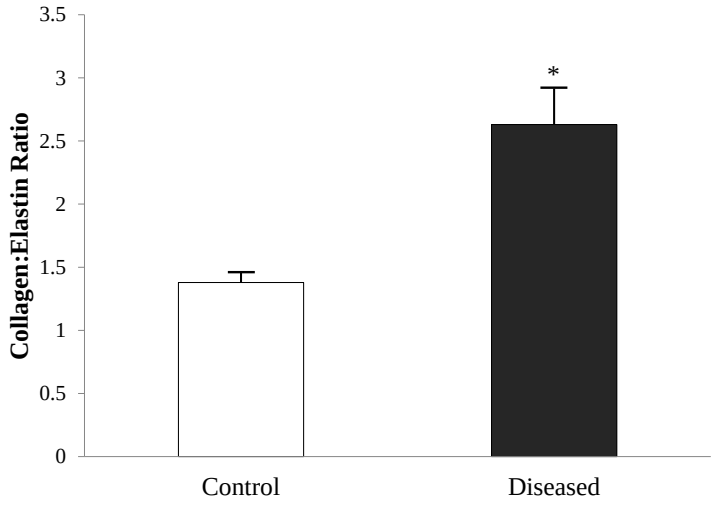

Fig. 3.16. Collagen to elastin ratio in control and diseased common iliac venous tissue using MPM. Figure shows grouped average for n = 6 dogs. Mean ± SE. $*$ $p < 0.05$ vs. control.

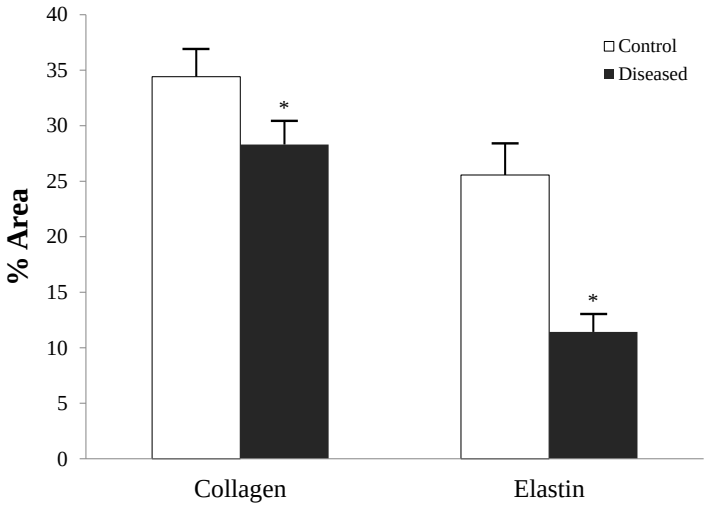

Fig. 3.17. Percent of collagen and elastin within the venous wall of control and diseased common iliac veins. Figure shows grouped average for n = 6 dogs. Mean ± SE. $*$ $p < 0.05$ vs. control.

4. DISCUSSION

Current knowledge of venous tissue, in both the healthy and the diseased states, is substantially behind the knowledge of arterial tissue. The basic concepts and investigation of vascular biomechanics pertaining to the arterial wall are well established, while the investigation of biomechanical properties of the venous tissue is limited. The investigations of the biomechanical properties of the venous wall that do exist, mainly focused on the remodeling of veins exposed to non-physiologic, static hypertension (i.e. gravitational loading) [8, 32, 33] or veins exposed to an arterial environment (i.e. high pressures and pulsatile flow) [30, 39, 69, 71]. In these studies, the biomechanical properties of the veins are obtained by using the existing principles and assumptions established in arterial wall mechanics. However, as discussed in Chapter 1, it is known that veins are hemodynamically, functionally, and structurally different from arteries. Thus, not all assumptions may directly translate. This thesis set out to test a key assumption, the incompressibility assumption, which is well established in arterial wall mechanics, but not tested in venous wall mechanics. Additionally, this thesis set out to expand the current knowledge of venous tissue by investigating the venous remodeling that occurs, both mechanically and structurally, when exposed to venous retrograde flow (reflux) and hypertension.

Venous retrograde flow (reflux) due to venous valve incompetence is the prevailing theory in the etiology of venous hypertension [6]. The primary objective of this thesis is to quantify the passive biomechanical response and structural remodeling of venous tissue subjected to chronic venous hypertension due to reflux. First, it was hypothesized that, if the venous wall was subjected to venous hypertension due to chronic venous reflux, then the passive mechanical properties of the venous tissue will remodel such that the tissue will become stiffer. Secondly, it was hypothesized that, if the venous wall was subjected to venous hypertension due to chronic venous reflux,

then the overall thickness of the wall would increase in addition to the composition of collagen and elastin in the wall changing. However, no model exists which is hemodynamically relevant to what is seen clinically. Thus, in order to investigate these hypotheses, a novel reflux induced hypertensive large animal model was implemented. The common iliac veins were investigated in this novel animal model using a novel experimental method.

4.1 Novelty

No studies have looked at the passive biomechanical properties of control or diseased canine common iliac veins. Prior to this study, venous research focused on the biomechanics of the vena cava [29,63,69,80], the femoral vein [30,31], and the saphenous vein [14,32,38–40,71,81]. However, workload and functional requirements of the veins are not consistent throughout the venous system [82]. Therefore, the biomechanical properties differ depending on the veins location within the venous vascular tree [83]. The variability in venous structure negates quantitative comparison of the data obtained in this thesis against existing data in the literature. However, the relationship and mechanical properties of venous tissue have been well established in other studies, focusing on other species (i.e. rabbits) and veins (i.e. femoral vein). The biomechanical data obtained using the novel experimental method, inflation-extension protocol combined with IVUS, was instead qualitatively compared to these established trends and relationships of the mechanical results (pressures-diameter and stress-strain) found in literature.

The passive mechanics of control and diseased canine common iliac veins were determined by integrating the conventional inflation-extension protocol with intravascular ultrasound (IVUS). Prior to this study, veins were assumed to be incompressible in order to analytically and experimentally simplify the problem [71]. The incompressibility assumption allowed for the inner diameters to be theoretically calculated using the loaded condition outer diameter and the zero stress condition thickness. However,

no material remains incompressible under all loads and conditions. Therefore, this assumption is not an exact representation of physics [28, 84]. Assumptions should be based primarily on the physics, not mathematical convenience. Using IVUS in conjunction with the conventional inflation-extension protocol allowed for the inner diameter to be directly measured in each loaded condition and the incompressibility assumption to be disregarded. Using the experimentally obtained inner and outer diameters, the actual change in wall volume was able to be calculated at each loaded condition.

If the wall of a vessel is incompressible, the calculated actual change in wall volume will always be equal to 1, despite the applied load. Experimentally, it was found that the mean volume change in arteries at physiologic length was not significantly different from 1. This finding supports the literature which has established that incompressibility is a reasonable assumption in arterial wall mechanics [28, 62, 85]. Additionally, this finding supports the initial hypothesis that if IVUS is integrated with the conventional inflation-extension protocol then the calculated mean volume change will be equal to 1 validating that the arterial wall is incompressible. Unlike arteries, the control veins did experience a mean volume change significantly lower than 1 (Figure 3.7). A decrease in volume indicates that water was expelled from the venous tissue during the loading procedure. This significant decrease in volume suggests that, under the loaded conditions studied, the venous wall is more permeable to water than the arterial wall. Permeability is the ability of the vessel wall to allow liquid to pass through it and is inversely proportional to the wall thickness [86]. A predominant structural difference between the veins and arteries is the overall thickness of the vessel wall [15]. This infers that the arterial wall has a lower permeability than the venous wall, since arteries are thicker than veins. This is supported by Sarelius et al. whom has demonstrated that the permeability of control arterioles is significantly lower than the permeability of control venules [87]. Thus, due to the veins higher permeability and resulting decrease in wall volume during the loading procedure, incompressibility is not a reasonable assumption in venous wall mechan-

ics, when studied in vitro; thus, disproving the hypothesis that the incompressibility assumption can be applied to venous wall mechanics.

Due to the significant decrease in wall volume and the increase in permeability, it is presumed that the in vitro observation (that the incompressibility assumption is not applicable to venous tissue) would also hold true in vivo. However, in this study the surrounding tissue was dissected away and the mechanical contribution and external forces exerted by the surrounding tissues in vivo were not considered [34, 88–90]. Therefore, the observation that the incompressibility assumption is not applicable to venous tissue may be a result of the experimental preparation since the external pressure, due to surrounding tissue was not accounted for [91]. In vitro, the external pressure exerted on the wall was always equal to or lower than the internal pressure. In vivo, the osmotic pressure due to the surrounding tissue will be higher, than in the in vitro studies, which may potentially be able to oppose water from being expelled from the venous tissue during the loaded condition. It is not known the degree to which the presence of external force will prevent volume change, but based off the decreases in wall volume and the higher wall permeability, observed in vitro; it seems unlikely the presence of external forces would render the venous wall incompressible.

A novel large animal model of chronic venous reflux was introduced to investigate the biomechanical and microstructural remodeling of the common iliac vein exposed to chronic venous reflux and hypertension. Chronic venous reflux was created by disrupting the chordae tendineae by pulling a cutting device retrograde across the tricuspid valve from the right ventricle to the right atrium producing an injured tricuspid valve. This model demonstrated that disruption of the chordae tendineae produces an immediate increase in mean right atrial pressure and maximum jugular venous pressure. Detectable reflux flow began immediately, and notable pulsatile venous flow was observed. An immediate increase in reflux mirrored the immediate change in the femoral venous pressure. After the creation of mean reflux, there was no significant change in reflux fraction or FVP throughout the entire eight week duration of the study. Contrary to what has been clinically seen in CVI and in

previous hypertensive models [24], there was no in vivo dilation, or contraction, of the inner lumen observed. This may be due to the time points studied as well as the flow conditions. IVUS measurements were not made in vivo at the eight week mark (euthanization), thus it could be possible that dilation occurred in the last four weeks. Additionally, the common iliac veins were exposed to a 3-fold increase in maximum pressure which was significant enough to induce remodeling, but not enough to induce dilatation or contraction. These findings support the initial hypothesis that when the tricuspid valve was removed; the resulting venous reflux would create a significant increase in pressure (venous hypertension).

When the wall volume change of the veins exposed to chronic venous reflux was experimentally calculated, it was found that these diseased veins act similarly to the control veins, such that changes in volume were significantly lower than 1 and different from the control arteries. Histological evaluation showed that the wall of diseased vein was significantly thicker than the wall of the control vein after eight weeks of chronic reflux. It has been previously stated that permeability is dependent on wall thickness. Thus, it can be expected that the thinner control common iliac veins were more permeable to water than the thicker diseased common iliac veins. The experimental results support this, showing the wall volume change observed in diseased veins is less severe than the wall volume change observed in control veins (Figure 3.7). Thus, diseased veins were found to be less incompressible than arteries, but not as compressible as control veins. This suggests that the microstructural remodeling (i.e. hypertrophy) due to chronic reflux and hypertension decreased the permeability of the vein wall.

4.2 Biomechanical and Microstructural Remodeling

The objective of biomechanics is to develop, adapt, and apply the laws, theories, and principles of mechanics to answer questions of clinical importance [28]. The biomechanical properties of vascular tissue and their underlying microstructure can

aid in the understanding of the basic function of the vessel as well as the development of disease pathology [40]. The biomechanical properties, at all loaded conditions, were determined experimentally using the zero stress condition as the reference configuration. All zero stress condition parameters were significantly different in diseased common iliac veins and control common iliac veins. The open angle of the diseased vein was significantly higher than the control vein. These findings signify that the residual stress in the diseased veins were higher than the control vein, implying there was more stress in the diseased vein wall. The physiologic stretch ratio of the control common iliac veins was found to be 1.62 ± 0.02 which is slightly lower than what has been found in the vena cava ($\sim$2) [63]. No difference was found between the physiologic stretch ratios of the diseased and control veins, which indicate that the vessel did not significantly remodel in the axial direction. It was proposed that the majority of remodeling occurred in the circumferential direction.

When the biomechanical properties were calculated, a leftward shift of the circumferential Kirchhoff stress-Green strain curve was observed in both control and diseased veins, as the axial stretch ratio was increased. It was found that veins became stiffer in the circumferential directions as axial load was increased. The circumferential stress-strain curves of the control and diseased veins both demonstrated the J-shaped behavior typical of soft tissue [12, 92]. The passive mechanical response of veins is contributed by elastin and collagen [93]. The low-strain stiffness reflected in the stress-strain curve is referred to as the toe region. The toe region is determined by the elastin content and microstructure. The high-strain stiffness, represented by the second linear region of the stress-strain curve, represents the pseudoelasticity of the material and is determined by the collagen fibers [12, 70]. The circumferential stress-strain curves show a pronounced transition from the toe region to the second linear region at a pressure of $\sim$20 mmHg in control veins. In diseased veins it was found that the pronounced transition from the toe region to the second linear region occurs at $\sim$15 mmHg. The pronounced transition from the toe region to the second linear region has been found to reflect the relatively inextensible collagen fibers coming into

play [31]. When the pronounced transition occurs at a lower pressure, a shorter toe region is produced. This implies that the collagen fibers were recruited and the elastin was no longer the determinate of stiffness at a lower pressure in diseased veins. Since the mechanical response is contributed by elastin and collagen, the circumferential stress-strain curves alone suggest that the collagen to elastin ratio increased as a result of chronic venous reflux and hypertension. Additionally, at a given axial load, the diseased circumferential stress- strain curve was uniformly shifted up and to the left, indicating that, at a given Kirchhoff stress, the resulting Green stain is lower in diseased veins than control veins. These findings support the hypothesis that veins stiffen and the composition of collagen and elastin in the wall changes when exposed to chronic venous reflux and hypertension.

The experimental circumferential stress-stain curves suggested that the collagen to elastin ratio increased as a result of chronic venous reflux and hypertension. MPM showed a significant increase in the collagen to elastin ratio due to chronic hypertension. This finding supports the initial assumption made based off the experimental circumferential stress-strain curves. However, it was found that the relative amount of collagen within the venous wall did not significantly change between control and diseased tissue. The significant increase in the collagen to elastin ratio was the result of a significant decrease in the relative amount of elastin within the venous wall. This finding is supported by results by Watts et al. which state that under chronic reflux and hypertension redistribution and reorganization of the extracellular matrix occurs, particularly altered collagen composition and diminished elastin content [4,29,94,95].

In order to validate the results found using MPM, the experimental collagen to elastin ratio as well as the morphology and microstructure of the control canine common iliac vein were compared with the findings of Zocalo et al. [83]. Zocalo et al. [83] measured the elastin and collagen in the vena cava and femoral vein of a sheep using the Cajal-Gallego staining method. Figure 4.1 shows the histological analysis done by Zocalo et al. in an ovine femoral vein. This histological analysis done in this study shows similarities to the morphological structure and microstructure seen

in Figure 3.14. The vena cava was found to have a collagen to elastin ratio of 1.69, while the femoral vein was found to have a collagen to elastin ratio of 1.04. Since the common iliac vein is physiologically between the vena cava and the femoral vein, a collagen to elastin ratio of 1.38 ± 0.08 is assumed reasonable. The initial hypothesis states that, if the venous wall was subjected to venous hypertension due to chronic venous reflux, then the overall thickness of the wall would increase in addition to the composition of collagen and elastin in the wall changing. The findings from the MPM confirmed that, when the venous wall was subjected to venous hypertension due to chronic venous reflux, the composition of collagen to elastin within the wall increased. A histological evaluation was performed in order to evaluate if the overall thickness of the wall also increased as a result of venous hypertension due to chronic venous reflux.

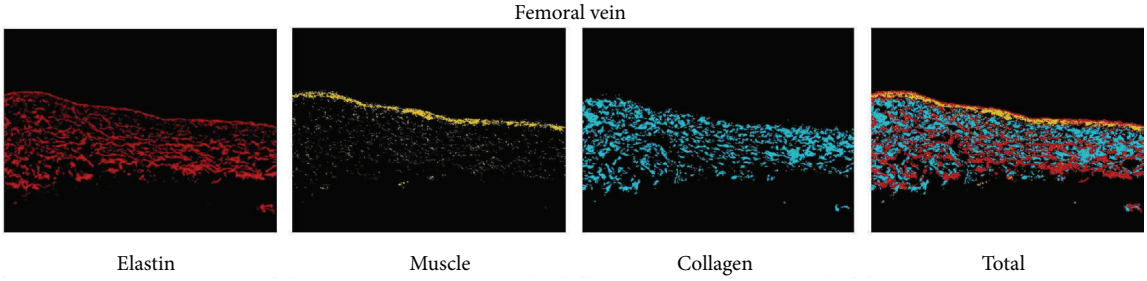

Fig. 4.1. Histological analysis in an ovine femoral vein show the location of each wall constituent. Left to right: elastin, smooth muscle, collagen, and the original image [83].

Histological results show that, in the no load condition, the total venous wall thickness and the intimal-medial thickness both significantly increased in response to chronic venous hypertension. Additionally, the pressure-diameter curves show that, when the inner and outer diameter curves for the control and diseased vessels at the same axial stretch ratio are plotted together, there was no significant shift of the diameter curves. This indicated that there was no visible dilation caused by eight

weeks of chronic reflux. However, the thickness curve is significantly shifted upwards after eight weeks of chronic reflux, indicating that in the loaded condition, the total venous wall thickened in response to chronic venous hypertension.

Wall hypertrophy is a mechanical adaption phenomenon seen in arterial walls in response to increased pressure [31]. Veins introduced into the arterial system for the use as a bypass graft exhibit similar adaptation mechanisms as arteries in response to hypertension [96]. When saphenous veins are introduced into the arterial system for use as a bypass graft, they experience a significant change in intraluminal pressure, blood flow and cyclic loading due to pulsatility [36]. Two structural changes occur when veins are exposed to arterial pressure and flow conditions: intimal hyperplasia and medial thickening. These two structural changes are a result of two different stimuli. Intimal hyperplasia is a result of abnormal flow characteristics at the blood-intima interface, while medial thickening is likely due to chronic high pressure [39]. It has been observed that when a vein is introduced into the arterial environment, the vein will first undergo thickening to restore the wall circumferential Cauchy stress to a normal value under hypertension. Several weeks later, the inner diameter will enlarge in response to blood flow changes, in order to restore shear stress to normal values [70].

Assuming that the common iliac vein remodels in a similar fashion as an arterialized vein, after eight weeks of chronic reflux and hypertension the circumferential Cauchy stress would be expected to have been reduced back to 7.86 $\pm$ 0.65 kPa (Figure 3.11). However, results show that the circumferential Cauchy stress did significantly decrease due to remodeling (24.09 $\pm$ 1.29 kPa), but not to the extent where the stress was reduced to the control (7.86 $\pm$ 0.65 kPa). Similarly, in vivo inner diameter measurements found no significant dilation of inner lumen due to two weeks of reflux. However, IVUS measurements were not made in vivo at the eight week mark, thus it could be possible that dilation occurred in the last four weeks. Using the inner diameter found at 20 mmHg at 100% physiologic length in the diseased vessel at the eight week mark, inner diameter (9.04 $\pm$ 0.38 mm) still indicates that no significant

dilation or contraction occurred due to eight weeks of chronic reflux (when compared to baseline: 10.14 ± 0.36 mm and four weeks: 10.07 ± 0.26 mm).

The common iliac veins were exposed to a 3-fold increase in maximum pressure (∼7 mmHg to ∼20 mmHg), a 2-fold increase in mean pressure (∼5 mmHg to ∼10 mmHg) for eight weeks, and an average mean reflux fraction of 26%. The PWV tracings indicate that the venous flow within the common iliac vein became pulsatile after the creation of reflux. The results suggest that the increase in pressure in response to chronic reflux were significant enough to induce medial thickening, and the flow characteristics at the blood-intima interface were significant enough to create intimal hyperplasia, but not enough to induce vessel dilation within the first 6 weeks. Thus, common iliac veins exposed to chronic venous reflux for eight weeks do not remodel in a similar fashion as arteries or veins introduced into the arterial system. These results suggest that remodeling laws of veins may be dependent upon the type and/or intensity of the biomechanical stimulus driving the remodeling process.

In summary, removal of the tricuspid valve created chronic venous reflux. As a result of venous reflux, the venous pressure within the common iliac vein chronically increased. In response to venous hypertension and reflux, the venous wall thickened and the elastin content within the venous wall decreased, producing a stiffer vein. When the vein stiffened, the vein became less compliant. Venous pathology develops when venous pressure is increased and the venous return of blood is impaired [3]. Reduction in the compliance of the vein impairs the venous return of blood. Coupled with venous reflux, venous blood starts to accumulate within the lower limbs, raising the blood pressure and causing the vein to distend. Results show that the common iliac veins of the animal model exhibited signs of hypertension and wall stiffening but did not show distension. However, it may be deduced that if this model was extended out to 3 months, distension of the veins will occur. Distension of the veins causes the venous valves to be incompetent. As the valves become incompetent, the venous pressure in surrounding tissue and capillaries rises. Increased venous hydrostatic pressure causes a shift in the venous hemodynamics with changes in the wall shear

stress. This initiates the inflammatory cascade [24], leading to the manifestation of the primary clinical indicators of CVI, which are dilated veins, edema, leg pain, and skin changes [3]. Thus, the venous remodeling due to the hypertension created by venous reflux implicates reflux as the prevailing theory in the etiology of venous hypertension.

4.3 Experimental Limitations of the Study

Certain limitations with the methodology of this study need acknowledgement. The effects of VSMCs on the mechanical properties and remodeling were neglected. It was assumed that the effects of the passive mechanical properties due to VSMCs were negligible and that the passive response results were solely from the mechanical properties of the elastin and collagen. VSMCs are known to play a role in the both passive and active mechanical properties, remodeling, and stress reduction of vascular walls due to hypertension [97]. Future studies should investigate the role of VSMCs associated with active as well as the passive biomechanical properties.

It was assumed that the axial stretch was unchanged during the inflation process. The axial changes during inflation were recorded using the digital camera images taken to compare the accuracy of IVUS. It was observed that the axial stretch during the inflation was small. Future improvements will allow tracking of movements in the axial direction using a video camera and tracking software.

IVUS was found to overestimate the outer diameter of both veins and arteries by 6.46% when compared with measurements made by the digital camera. By using IVUS, the ability to directly measure the inner diameter was gained, but the accuracy of the outer diameter measurement was slightly compromised. A more true measurement of outer diameter would be found using the conventional digital camera method. However, when comparing thicknesses, diameters, and mechanical properties obtained from the IVUS images to past studies, the slight overestimation does not significantly affect or skew the biomechanical analysis. Future advances should

integrate the tracking software and digital camera to measure outer diameter and IVUS for inner diameter.

In regards to the mathematical modeling aspect of this study, the exponential Fung-type SEF was fit to the experimental mechanical data. Two general approaches exist in order to describe the mechanical behavior of soft tissue using SEFs: phenomenological and structural. In phenomenological approaches, the mathematical expression is chosen to reflect the biomechanical behavior of the wall, but the material constants do not necessarily have any physical meaning. In structural approaches, each wall constituents individual contribution to the SEF is accounted for and the material constants correspond to some physical properties of the tissue (i.e. wall fractions of elastin and collagen) [72]. The exponential Fung-type SEF uses the phenomenological approach to describe the mechanical behavior of the venous tissue. Thus, the obtained model and material constants in this study mathematically express the results of the observed phenomenon, but does not correspond to physical properties of the venous tissues microstructure.

Lastly, MPM imaging is a semi-quantitative analytical approach to obtaining the wall fractions of elastin and collagen. Future improvements will introduce collagen and elastin assays to quantitatively analyze the wall fractions of elastin and collagen. A fully quantitative approach allows for very little bias and is purely empirical.

4.4 Future Directions

To further strengthen the predictability of the biomechanical data presented, a SEF that uses the structural approach should be fit to the biomechanical properties and microstructure of the control and diseased common iliac veins [98]. The structural approach of Zulliger et al. [99] would take into account the collagen and elastin, which are the two major wall components bearing load in the passive state. Unlike in the exponential Fung-type model, the parameters of this model will provide physical

significance and yield realistic values, as well as provide a good description of the passive biomechanical properties of the wall.

The biomechanical properties of venous tissue and their underlying microstructure can aid in the understanding of the basic function of the vein as well as the development of disease pathology. After eight weeks of chronic reflux the circumferential Cauchy stress was not reduced due to hypertrophy to the degree that is seen in arteries. This may be a result of a longer time period which might have been needed for it to return to normal or restoration of circumferential Cauchy stress may not be the biological target for remodeling of the vein in these conditions (venous reflux and venous hypertension). Additionally, in response to venous reflux and hypertension, the venous wall thickened and the elastin content within the venous wall decreased, producing a stiffer vein. When the vein stiffened the vein became less compliant. Reduction in the compliance of the vein impairs the venous return of blood. Coupled with venous reflux, venous blood starts to accumulate within the lower limbs raising the blood pressure and causing the vein to distend. Results show that the common iliac veins of the animal model exhibited signs of hypertension and wall stiffening, but did not show distension. These results indicate the development of venous pathology, but not manifestation of CVI. In the original animal model, the common iliac veins studied experienced chronic venous reflux for eight weeks. Further studies should be done obtaining the biomechanical properties and microstructural data for common iliac veins which have experienced chronic venous reflux for 3 months or longer. This would tell if a longer time period is needed to restore circumferential Cauchy stress to normal values, as well as to exhibit clinical indicators of CVI.

Additional studies should be done to validate that the incompressibility assumption is invalid in venous tissue. If this observation is validated, then the inflation-extension protocol integrated with IVUS presented in this thesis may be a valuable tool, particularly when coupled with direct external diameter measurements. Using this methodology to investigate the mechanical properties of the veins further down the venous tree (i.e. the femoral vein or the popliteal) in the reflux induced venous

hypertensive large animal model would provide insight into the progression of venous pathology. Additionally, further investigation needs to be done to explain and quantify the loss of venous wall volume due to loading. It is hypothesized that the loss of volume is due to the permeability differences between veins and arteries; however, this hypothesize was derived from observations made on arteriole and venules. Studies should be performed to test this hypothesis.

Future studies should also address the venous remodeling and biomechanical properties of common iliac veins effected by post-thrombotic syndrome and the consequences of stenting [100]. Post-thrombotic syndrome (PTS) is a manifestation of venous insufficiency following a deep vein thrombosis (DVT). PTS is the consequence of venous hypertension which leads to impaired venous return [100]. The two main mechanisms associated with PTS are persistent venous obstruction and venous reflux [100], but the symptoms are believed to be caused by outflow obstruction. Balloon dilation and insertion of a stent are used to correct venous obstruction [101]. Valuable insight could be gained comparing the venous remodeling in response to venous reflux, the venous remodeling in response to venous obstruction, and the venous remodeling and biomechanical properties of the venous wall after venous stenting.

Lastly, results show that in response to venous reflux and hypertension the venous wall thickened and the elastin content within the venous wall decreased, producing a stiffer vein. Further studies should investigate if the stiffening (i.e. remodeling) may be reversed. If the remodeling may be reversed (i.e. by eliminating reflux, pulsatile flow and/or hypertension) at what point does it become irreversible. Answers to these questions may have clinical importance especially in relation to CVI therapies (i.e. venous valve, stents, and external compression).

4.5 Contributions

The original conception and design of using IVUS in the inflation-extension protocol was presented to the author by Dr. Ghassan Kassab and Dr. Zachary Berwick.

From there, the author adapted and built upon the initial concept to create what you see today. The author executed all data collection and analysis presented. All methods stated, the author performed with the exception of the animal model and the running of the MPM. She did not conceptualize and/or create the large animal model used throughout this thesis. All credit in regards to the animal model goes to Dr. Zachary Berwick, Mr. Joshua Krieger, Dr. Ghassan Kassab, 3DT, and Cook Medical. In addition, all surgical procedures pertaining to the animal model were performed by Dr. Zachary Berwick and Mr. Joshua Krieger. All PWV tracings were obtained through a combination effort of Dr. Zachary Berwick or Mr. Joshua Krieger running the ultrasound transducer probe while either Miss Arika Kemp or the author ran the ultrasound machine and captured the data. Lastly, Dr. Huan Chen ran the MPM machine. While the author was present, Dr. Huan Chen controlled the settings and captured the data/images.

All further experiments, data collection, analysis, interpretations, and statistical analysis were performed by the author. During all three animal procedures she collected and analyzed all pressure and IVUS data and monitored the ECG, RAP, RVP, and JVP. She also analyzed the PWV images and obtained the reflux fraction. She harvested all vascular tissue, fixed segments of venous tissue for histology and MPM, and cleaned loosely connected tissue from the vessels prior to biomechanical testing. For the biomechanical testing she made the 3 mM EGTA solution, mounted the vessel, and solely ran the inflation-extension protocol. After the biomechanical tests she cut the three rings, relieved the residual stress, and analyzed the images to obtain the open angle and zero-stress condition inner and outer diameters. All IVUS images obtained and used in this thesis were taken and measured by her. She performed all the biomechanical analysis. The Fung-type exponential model was fit to the biomechanical data and the material constants were obtained by her. In regards to the histology, she rinsed the vessel rings in buffer solution, processed the tissue by dehydration, and embedded the segments in glycol methacrylate. The author also cut the embedded segments with a conventional microtome, mounted them on glass slides, and stained

them with toluidine blue. She photographed the histological sections and obtained the wall thickness measurements. The slides for MPM were prepared by the author. She froze the segments in Neg-50 gel, cut the sections using a conventional cryostat, mounted them on glass slides, surrounded them with solution (which I made), and encased them with a cover slip. All analysis and interpretations obtained from the MPM images was performed by the author. Lastly, the writing of this thesis was done by Miss Margaret Brass with continuous guidance and editing by Dr. Mark Svendsen and Dr. Zachary Berwick.

5. CONCLUSION

Using IVUS in conjunction with the conventional inflation-extension protocol allows for the incompressibility assumption to be disregarded. This study shows that integrating IVUS with the conventional inflation-extension protocol verifies the premise that the incompressibility assumption can be applied to arterial wall mechanics. However, results found incompressibility to not be a reasonable assumption in venous wall mechanics. The conventional inflation-extension protocol in conjunction with IVUS was utilized to investigate the passive biomechanical response and structural remodeling of the common iliac vein subjected to chronic venous reflux and hypertension.

Venous retrograde flow (reflux) is the prevailing theory in the etiology of venous hypertension. This study shows that removal of the tricuspid valve produced chronic venous reflux which additionally led to an increase in venous pressure (venous hypertension). Biomechanical results indicate that the veins stiffened and became less compliant when exposed to eight weeks of chronic venous reflux. The mechanical stiffening was found to be a result of wall hypertrophy as well as an increase in the collagen to elastin ratio. The increase in collagen to elastin ratio was found to be a direct result of the decrease in relative amount of elastin within the venous wall. The venous wall thickening resulted in the reduction of the circumferential Cauchy stress. However, after eight weeks of chronic reflux, the circumferential Cauchy stress was not restored to control levels due to wall thickening and the elasticity and compliance of the wall were found to decrease. The remodeling phenomena found in the vein were not similar to those observed in hypertensive arteries or bypass graft veins. These results suggest that remodeling laws of veins may be dependent upon the type and/or intensity of the biomechanical stimulus driving the remodeling process.

This study provides a biomechanical understanding of veins with predisposition for CVI. The biomechanical and morphological characterization of venous remodeling

is clinically relevant as venous hypertension and impairment of venous return have been associated with the onset of venous insufficiency. Therefore, development of a therapeutic rationale for prevention and future reduction of CVI must consider the biomechanical response and structural remodeling of the venous wall in response to venous reflux and hypertension.

LIST OF REFERENCES

LIST OF REFERENCES

[1] K. S. Saladin and L. Miller, *Anatomy & physiology*. McGraw-Hill, 1998.

[2] M. H. Meissner, P. Gloviczki, J. Bergan, R. L. Kistner, N. Morrison, F. Pannier, P. J. Pappas, E. Rabe, S. Raju, and J. L. Villavicencio, "Primary chronic venous disorders," *Journal of vascular surgery*, vol. 46, no. 6, pp. S54–S67, 2007.

[3] R. T. Eberhardt and J. D. Raffetto, "Chronic venous insufficiency," *Circulation*, vol. 111, no. 18, pp. 2398–2409, 2005.

[4] J. L. Beebe-Dimmer, J. R. Pfeifer, J. S. Engle, and D. Schottenfeld, "The epidemiology of chronic venous insufficiency and varicose veins," *Annals of epidemiology*, vol. 15, no. 3, pp. 175–184, 2005.

[5] R. Klabunde, *Cardiovascular physiology concepts*. Lippincott Williams & Wilkins, 2011.

[6] V. B. Flow, "The venous valve and primary chronic venous disease," *The Venous Valve and Primary Chronic Venous Disease*, vol. 30, no. 2, p. 116, 2008.

[7] J. J. Bergan, G. W. Schmid-Schönbein, P. D. C. Smith, A. N. Nicolaides, M. R. Boisseau, and B. Eklof, "Chronic venous disease," *New England Journal of Medicine*, vol. 355, no. 5, pp. 488–498, 2006.

[8] E. Monos, M. Lóránt, G. Dörnyei, V. Bérczi, and G. Nádasy, "Long-term adaptation mechanisms in extremity veins supporting orthostatic tolerance," *Physiology*, vol. 18, no. 5, pp. 210–214, 2003.

[9] F. A. Schneider, I. R. Siska, and J. A. Avram, *Clinical physiology of the venous system*, vol. 15. Taylor & Francis US, 2003.

[10] R. P. Vito and S. A. Dixon, "Blood vessel constitutive models-1995-2002," *Annual review of biomedical engineering*, vol. 5, no. 1, pp. 413–439, 2003.

[11] R. J. Dilley, J. K. McGeachie, and F. J. Prendergast, "A review of the histologic changes in vein-to-artery grafts, with particular reference to intimal hyperplasia," *Archives of surgery*, vol. 123, no. 6, p. 691, 1988.

[12] J. S. Rossmann, "Elastomechanical properties of bovine veins," *Journal of the mechanical behavior of biomedical materials*, vol. 3, no. 2, pp. 210–215, 2010.

[13] S. Glagov, R. Vito, D. P. Giddenst, and C. K. Zarins, "Micro-architecture and composition of artery walls: relationship to location, diameter and the distribution of mechanical stress," *Journal of Hypertension*, vol. 10, pp. S101–S104, 1992.

[14] W. Stooker, M. Gök, P. Sipkema, H. W. Niessen, A. Baidoshvili, N. Westerhof, E. K. Jansen, C. R. Wildevuur, and L. Eijsman, "Pressure-diameter relationship in the human greater saphenous vein," *The Annals of thoracic surgery*, vol. 76, no. 5, pp. 1533–1538, 2003.

[15] E. O. Attinger, "Wall properties of veins," *Biomedical Engineering, IEEE Transactions on*, no. 4, pp. 253–261, 1969.

[16] X. Guo, Y. Liu, and G. S. Kassab, "Diameter-dependent axial prestretch of porcine coronary arteries and veins," *Journal of applied physiology*, vol. 112, no. 6, pp. 982–989, 2012.

[17] I. C. Valencia, A. Falabella, R. S. Kirsner, and W. H. Eaglstein, "Chronic venous insufficiency and venous leg ulceration," *Journal of the American Academy of Dermatology*, vol. 44, no. 3, pp. 401–424, 2001.

[18] M. H. Meissner, G. Moneta, K. Burnand, P. Gloviczki, J. M. Lohr, F. Lurie, M. A. Mattos, R. B. McLafferty, G. Mozes, R. B. Rutherford, *et al.*, "The hemodynamics and diagnosis of venous disease," *Journal of vascular surgery*, vol. 46, no. 6, pp. S4–S24, 2007.

[19] T. Phillips, B. Stanton, A. Provan, and R. Lew, "A study of the impact of leg ulcers on quality of life: financial, social, and psychologic implications," *Journal of the American Academy of Dermatology*, vol. 31, no. 1, pp. 49–53, 1994.

[20] C. Bolcal, M. Sargin, I. Mataraci, H. Iyem, S. Doganci, S. Kilic, V. Temizkan, U. Demirkilic, and H. Tatar, "Concomitance of varicoceles and chronic venous insufficiency in young males," *Phlebology*, vol. 21, no. 2, pp. 65–69, 2006.

[21] N. Labropoulos, J. Tiongson, L. Pryor, A. K. Tassiopoulos, S. S. Kang, M. Ashraf Mansour, and W. H. Baker, "Definition of venous reflux in lower-extremity veins," *Journal of vascular surgery*, vol. 38, no. 4, pp. 793–798, 2003.

[22] N. Labropoulos, A. D. Giannoukas, A. N. Nicolaides, M. Veller, M. Leon, and N. Volteas, "The role of venous reflux and calf muscle pump function in non-thrombotic chronic venous insufficiency: correlation with severity of signs and symptoms," *Archives of Surgery*, vol. 131, no. 4, p. 403, 1996.

[23] H. M. Atta, "Varicose veins: role of mechanotransduction of venous hypertension," *International journal of vascular medicine*, vol. 2012, 2012.

[24] L. Pascarella, G. W. Schmid-Schönbein, and J. Bergan, "An animal model of venous hypertension: the role of inflammation in venous valve failure," *Journal of vascular surgery*, vol. 41, no. 2, pp. 303–311, 2005.

[25] J. J. Bergan, L. Pascarella, and G. W. Schmid-Schönbein, "Pathogenesis of primary chronic venous disease: Insights from animal models of venous hypertension," *Journal of vascular surgery*, vol. 47, no. 1, pp. 183–192, 2008.

[26] M. C. Dalsing, A. J. Zukowski, J. L. Unthank, S. G. Lalka, A. P. Sawchuk, and D. E. Cikrit, "Details of a canine venous insufficiency model," *Investigative Surgery*, vol. 7, no. 2, pp. 85–93, 1994.

[27] M. C. Dalsing, J. J. Ricotta, T. Wakefield, T. G. Lynch, and K. Ouriel, "Animal models for the study of lower extremity chronic venous disease: lessons learned and future needs," *Annals of vascular surgery*, vol. 12, no. 5, pp. 487–494, 1998.

[28] J. D. Humphrey, *Cardiovascular solid mechanics: cells, tissues, and organs*. Springer, 2002.

[29] S. W. Watts, C. Rondelli, K. Thakali, X. Li, B. Uhal, M. H. Pervaiz, R. E. Watson, and G. D. Fink, "Morphological and biochemical characterization of remodeling in aorta and vena cava of doca-salt hypertensive rats," *American Journal of Physiology-Heart and Circulatory Physiology*, vol. 292, no. 5, pp. H2438–H2448, 2007.

[30] K. Hayashi and T. Naiki, "Adaptation and remodeling of vascular wall; biomechanical response to hypertension," *Journal of the mechanical behavior of biomedical materials*, vol. 2, no. 1, pp. 3–19, 2009.

[31] K. Hayashi, K. Mori, and H. Miyazaki, "Biomechanical response of femoral vein to chronic elevation of blood pressure in rabbits," *American Journal of Physiology-Heart and Circulatory Physiology*, vol. 53, no. 2, p. H511, 2003.

[32] E. Monos, S. J. Contney, A. Cowley, and W. J. Stekiel, "Effect of long-term tilt on mechanical and electrical properties of rat saphenous vein," *American Journal of Physiology-Heart and Circulatory Physiology*, vol. 256, no. 4, pp. H1185–H1191, 1989.

[33] E. Monos, K. Kauser, S. Contney, A. Cowley Jr, and W. Stekiel, "Biomechanical and electrical responses of normal and hypertensive veins to short-term pressure increases," in *Cellular Aspects of Hypertension*, pp. 51–57, Springer, 1991.

[34] J. S. Choy and G. Kassab, "Non-uniformity of axial and circumferential remodeling of large coronary veins in response to ligation," *Journal of Biomechanics*, vol. 39, p. S316, 2006.

[35] J. S. Choy and G. S. Kassab, "A novel strategy for increasing wall thickness of coronary venules prior to retroperfusion," *American Journal of Physiology-Heart and Circulatory Physiology*, vol. 291, no. 2, pp. H972–H978, 2006.

[36] D. A. Severyn, S. C. Muluk, and D. A. Vorp, "The influence of hemodynamics and wall biomechanics on the thrombogenicity of vein segments perfused in vitro," *Journal of Surgical Research*, vol. 121, no. 1, pp. 31–37, 2004.

[37] E. Monos, V. Berczi, and G. Nadasy, "Local control of veins: biomechanical, metabolic, and humoral aspects," *Physiological reviews*, vol. 75, no. 3, pp. 611–666, 1995.

[38] C. D. Owens, N. Wake, J. G. Jacot, M. Gerhard-Herman, P. Gaccione, M. Belkin, M. A. Creager, and M. S. Conte, "Early biomechanical changes in lower extremity vein graftsdistinct temporal phases of remodeling and wall stiffness," *Journal of vascular surgery*, vol. 44, no. 4, pp. 740–746, 2006.

[39] P. B. Dobrin, F. N. Littooy, J. Golan, B. Blakeman, and J. Fareed, "Mechanical and histologic changes in canine vein grafts," *Journal of Surgical Research*, vol. 44, no. 3, pp. 259–265, 1988.

[40] D. P. Sokolis, "Passive mechanical properties and constitutive modeling of blood vessels in relation to microstructure," *Medical & biological engineering & computing*, vol. 46, no. 12, pp. 1187–1199, 2008.

[41] G. S. Kassab, "Biomechanics of the cardiovascular system: the aorta as an illustratory example," *Journal of The Royal Society Interface*, vol. 3, no. 11, pp. 719–740, 2006.

[42] C. Chuong and Y. Fung, "Residual stress in arteries," in *Frontiers in Biomechanics*, pp. 117–129, Springer, 1986.

[43] J. C. Jacobsen and N.-H. Holstein-Rathlou, "A life under pressure: circumferential stress in the microvascular wall," *Basic & clinical pharmacology & toxicology*, vol. 110, no. 1, pp. 26–34, 2012.

[44] Y. Fung and S. Liu, "Strain distribution in small blood vessels with zero-stress state taken into consideration," *American Journal of Physiology-Heart and Circulatory Physiology*, vol. 262, no. 2, pp. H544–H552, 1992.

[45] X. Guo and G. S. Kassab, "Distribution of stress and strain along the porcine aorta and coronary arterial tree," *American Journal of Physiology-Heart and Circulatory Physiology*, vol. 286, no. 6, pp. H2361–H2368, 2004.

[46] Y. Fung and S. Liu, "Change of residual strains in arteries due to hypertrophy caused by aortic constriction.," *Circulation Research*, vol. 65, no. 5, pp. 1340–1349, 1989.

[47] A. Rachev and S. Greenwald, "Residual strains in conduit arteries," *Journal of biomechanics*, vol. 36, no. 5, pp. 661–670, 2003.

[48] Y. Fung, "What are the residual stresses doing in our blood vessels?," *Annals of biomedical engineering*, vol. 19, no. 3, pp. 237–249, 1991.

[49] Y. Fung and S. Liu, "Changes of zero-stress state of rat pulmonary arteries in hypoxic hypertension," *Journal of Applied Physiology*, vol. 70, no. 6, pp. 2455–2470, 1991.

[50] S. G. Sassani, A. Theofani, S. Tsangaris, and D. P. Sokolis, "Time-course of venous wall biomechanical adaptation in pressure and flow-overload: Assessment by a microstructure-based material model," *Journal of biomechanics*, vol. 46, no. 14, pp. 2451–2462, 2013.

[51] K. C. McGilvray, R. Sarkar, K. Nguyen, and C. M. Puttlitz, "A biomechanical analysis of venous tissue in its normal and post-phlebitic conditions," *Journal of biomechanics*, vol. 43, no. 15, pp. 2941–2947, 2010.

[52] A. H. Moreno, A. I. Katz, L. D. Gols, and R. Reddy, "Mechanics of distension of dog veins and other very thin-walled tubular structures," *Circulation research*, vol. 27, no. 6, pp. 1069–1080, 1970.

[53] N. Gundiah, M. B Ratcliffe, and L. A Pruitt, "Determination of strain energy function for arterial elastin: experiments using histology and mechanical tests," *Journal of biomechanics*, vol. 40, no. 3, pp. 586–594, 2007.

[54] M. Hasegawa, "Rheological properties and wall structures of large veins.," *Biorheology*, vol. 20, no. 5, pp. 531–545, 1982.

[55] Y. Fung, "Structure and stress-strain relationship of soft tissues," *American Zoologist*, vol. 24, no. 1, pp. 13–22, 1984.

[56] A. Sverdlik and Y. Lanir, "Time-dependent mechanical behavior of sheep digital tendons, including the effects of preconditioning," *Journal of biomechanical engineering*, vol. 124, no. 1, pp. 78–84, 2002.

[57] C. Wang, M. Garcia, X. Lu, Y. Lanir, and G. S. Kassab, "Three-dimensional mechanical properties of porcine coronary arteries: a validated two-layer model," *American Journal of Physiology-Heart and Circulatory Physiology*, vol. 291, no. 3, pp. H1200–H1209, 2006.

[58] G. Sommer, P. Regitnig, L. Költringer, and G. A. Holzapfel, "Biaxial mechanical properties of intact and layer-dissected human carotid arteries at physiological and supraphysiological loadings," *American Journal of Physiology-Heart and Circulatory Physiology*, vol. 298, no. 3, pp. H898–H912, 2010.

[59] E. Gultova, L. Horny, and H. Chlup, "A comparison between the exponential and limiting fiber extensibility pseudo-elastic model for the mullins effect in arterial tissue," *Journal of Theoretical and Applied Mechanics*, vol. 49, pp. 1203–1216, 2011.

[60] Y. Fung, K. Fronek, and P. Patitucci, "Pseudoelasticity of arteries and the choice of its mathematical expression," *American Journal of Physiology-Heart and Circulatory Physiology*, vol. 237, no. 5, pp. H620–H631, 1979.

[61] Y. Fung, "Elasticity of soft tissues in simple elongation.," *The American journal of physiology*, vol. 213, no. 6, p. 1532, 1967.

[62] C. Chuong and Y. Fung, "Compressibility and constitutive equation of arterial wall in radial compression experiments," *Journal of biomechanics*, vol. 17, no. 1, pp. 35–40, 1984.

[63] H. W. Weizsäcker, "Passive elastic properties of the rat abdominal vena cava," *Pflügers Archiv*, vol. 412, no. 1-2, pp. 147–154, 1988.

[64] J. De Mey and P. Vanhoutte, "Heterogeneous behavior of the canine arterial and venous wall. importance of the endothelium.," *Circulation research*, vol. 51, no. 4, pp. 439–447, 1982.

[65] J. Zhou and Y. Fung, "The degree of nonlinearity and anisotropy of blood vessel elasticity," *Proceedings of the National Academy of Sciences*, vol. 94, no. 26, pp. 14255–14260, 1997.

[66] J. C. Debes and Y. Fung, "Biaxial mechanics of excised canine pulmonary arteries," *American Journal of Physiology-Heart and Circulatory Physiology*, vol. 269, no. 2, pp. H433–H442, 1995.

[67] J. Cheung and C. Hsiao, "Nonlinear anisotropic viscoelastic stresses in blood vessels," *Journal of biomechanics*, vol. 5, no. 6, pp. 607–619, 1972.

[68] G. A. Holzapfel and R. W. Ogden, "On planar biaxial tests for anisotropic nonlinearly elastic solids. a continuum mechanical framework," *Mathematics and mechanics of solids*, vol. 14, no. 5, pp. 474–489, 2009.

[69] G. W. Desch and H. W. Weizsäcker, "A model for passive elastic properties of rat vena cava," *Journal of biomechanics*, vol. 40, no. 14, pp. 3130–3145, 2007.

[70] E. P. Kritharis, J. D. Kakisis, A. T. Giagini, T. Manos, N. Stergiopulos, S. Tsangaris, and D. P. Sokolis, "Biomechanical, morphological and zero-stress state characterization of jugular vein remodeling in arteriovenous fistulas for hemodialysis," *Biorheology*, vol. 47, no. 5, pp. 297–319, 2010.

[71] R. Wesly, R. N. Vaishnav, J. Fuchs, D. J. Patel, and J. Greenfield, "Static linear and nonlinear elastic properties of normal and arterialized venous tissue in dog and man.," *Circulation research*, vol. 37, no. 4, pp. 509–520, 1975.

[72] R. Rezakhaniha and N. Stergiopulos, "A structural model of the venous wall considering elastin anisotropy," *Journal of biomechanical engineering*, vol. 130, no. 3, p. 031017, 2008.

[73] A. Rachev and K. Hayashi, "Theoretical study of the effects of vascular smooth muscle contraction on strain and stress distributions in arteries," *Annals of biomedical engineering*, vol. 27, no. 4, pp. 459–468, 1999.

[74] G. A. Holzapfel, T. C. Gasser, and R. W. Ogden, "A new constitutive framework for arterial wall mechanics and a comparative study of material models," *Journal of elasticity and the physical science of solids*, vol. 61, no. 1-3, pp. 1–48, 2000.

[75] A. Y. Lee and H.-C. Han, "A nonlinear thin-wall model for vein buckling," *Cardiovascular Engineering and Technology*, vol. 1, no. 4, pp. 282–289, 2010.

[76] M. E. Valentinuzzi and A. K. Kohen, "Laplace's law: What it is about, where it comes from, and how it is often applied in physiology [retrospectroscope]," *Pulse, IEEE*, vol. 2, no. 4, pp. 74–84, 2011.

[77] Y. Fung and S. Liu, "Determination of the mechanical properties of the different layers of blood vessels in vivo," *Proceedings of the National Academy of Sciences*, vol. 92, no. 6, pp. 2169–2173, 1995.

[78] M. Carboni, G. W. Desch, and H. W. Weizsäcker, "Passive mechanical properties of porcine left circumflex artery and its mathematical description," *Medical engineering & physics*, vol. 29, no. 1, pp. 8–16, 2007.

[79] H. Chen, Y. Liu, M. N. Slipchenko, X. Zhao, J.-X. Cheng, and G. S. Kassab, "The layered structure of coronary adventitia under mechanical load," *Biophysical journal*, vol. 101, no. 11, pp. 2555–2562, 2011.

[80] Y. Lee, Y. Naito, H. Kurobe, C. Breuer, and J. Humphrey, "Biaxial mechanical properties of the inferior vena cava in c57bl/6 and cb-17 scid/bg mice," *Journal of biomechanics*, vol. 46, no. 13, pp. 2277–2282, 2013.

[81] J. G. Jacot, I. Abdullah, M. Belkin, M. Gerhard-Herman, P. Gaccione, J. F. Polak, M. C. Donaldson, A. D. Whittemore, and M. S. Conte, "Early adaptation of human lower extremity vein grafts: wall stiffness changes accompany geometric remodeling," *Journal of vascular surgery*, vol. 39, no. 3, pp. 547–555, 2004.

[82] Z. Krasiński, P. Biskupski, Ł. Dzieciuchowicz, E. Kaczmarek, B. Krasińska, R. Staniszewski, K. Pawlaczyk, M. Stanisić, P. Majewski, and W. Majewski, "The influence of elastic components of the venous wall on the biomechanical properties of different veins used for arterial reconstruction," *European Journal of Vascular and Endovascular Surgery*, vol. 40, no. 2, pp. 224–229, 2010.

[83] Y. Zócalo, D. Bia, E. I. Cabrera-Fischer, S. Wray, C. Galli, and R. L. Armentano, "Structural and functional properties of venous wall: Relationship between elastin, collagen, and smooth muscle components and viscoelastic properties," *ISRN Physiology*, vol. 2013, 2013.

[84] F. Di Puccio, S. Celi, and P. Forte, "Review of experimental investigations on compressibility of arteries and introduction of a new apparatus," *Experimental mechanics*, vol. 52, no. 7, pp. 895–902, 2012.

[85] T. E. Carew, R. N. Vaishnav, and D. J. Patel, "Compressibility of the arterial wall," *Circulation Research*, vol. 23, no. 1, pp. 61–68, 1968.

[86] G. A. Truskey, F. Yuan, and D. F. Katz, *Transport phenomena in biological systems*. Pearson/Prentice Hall Upper Saddle River NJ:, 2004.

[87] I. H. Sarelius, J. M. Kuebel, J. Wang, and V. H. Huxley, "Macromolecule permeability of in situ and excised rodent skeletal muscle arterioles and venules.," *American journal of physiology. Heart and circulatory physiology*, vol. 290, no. 1, p. H474, 2006.

[88] Y. Liu, W. Zhang, and G. S. Kassab, "Effects of myocardial constraint on the passive mechanical behaviors of the coronary vessel wall," *American Journal of Physiology-Heart and Circulatory Physiology*, vol. 294, no. 1, pp. H514–H523, 2008.

[89] P. Boutouyrie, Y. Bézie, P. Lacolley, P. Challande, P. Chamiot-Clerc, A. Benetos, J. F. R. de la Faverie, M. Safar, and S. Laurent, "In vivo/in vitro comparison of rat abdominal aorta wall viscosity influence of endothelial function," *Arteriosclerosis, thrombosis, and vascular biology*, vol. 17, no. 7, pp. 1346–1355, 1997.

[90] I. Masson, P. Boutouyrie, S. Laurent, J. D. Humphrey, and M. Zidi, "Characterization of arterial wall mechanical behavior and stresses from human clinical data," *Journal of biomechanics*, vol. 41, no. 12, pp. 2618–2627, 2008.

[91] L. J. Brossollet and R. P. Vito, "An alternate formulation of blood vessel mechanics and the meaning of the¡ i¿ in vivo¡/i¿ property," *Journal of biomechanics*, vol. 28, no. 6, pp. 679–687, 1995.

[92] G. A. Holzapfel, "Biomechanics of soft tissue," *The handbook of materials behavior models*, vol. 3, pp. 1049–1063, 2001.

[93] J. T. Apter and E. Marquez, "A relation between hysteresis and other visco elastic properties of some biomaterials.," *Biorheology*, vol. 5, no. 4, pp. 285–301, 1968.

[94] J. Travers, C. Brookes, J. Evans, D. Baker, C. Kent, G. Makin, and T. Mayhew, "Assessment of wall structure and composition of varicose veins with reference to collagen, elastin and smooth muscle content," *European journal of vascular and endovascular surgery*, vol. 11, no. 2, pp. 230–237, 1996.

[95] M. M. Naim and M. A. Elsharawy, "Histological assessment of the long saphenous vein in normal and varicose veins," *The Egyptian journal of histology*, vol. 28, pp. 281–290, 2005.

[96] R. J. Gusic, M. Petko, R. Myung, J. William Gaynor, and K. J. Gooch, "Mechanical properties of native and ex vivo remodeled porcine saphenous veins," *Journal of biomechanics*, vol. 38, no. 9, pp. 1770–1779, 2005.

[97] J. M. Price, P. Patitucci, and Y. C. Fung, "Mechanical properties of resting taenia coli smooth muscle," *American Journal of Physiology-Cell Physiology*, vol. 236, no. 5, pp. C211–C220, 1979.

[98] A. Agianniotis, R. Rezakhaniha, and N. Stergiopulos, "A structural constitutive model considering angular dispersion and waviness of collagen fibres of rabbit facial veins," *Biomedical engineering online*, vol. 10, no. 1, p. 18, 2011.

[99] M. A. Zulliger, P. Fridez, K. Hayashi, and N. Stergiopulos, "A strain energy function for arteries accounting for wall composition and structure," *Journal of biomechanics*, vol. 37, no. 7, pp. 989–1000, 2004.

[100] H. I. Saba and H. R. Roberts, *Hemostasis and Thrombosis: Practical Guidelines in Clinical Management*. John Wiley & Sons, 2014.

[101] P. Neglen, M. Berry, and S. Raju, "Endovascular surgery in the treatment of chronic primary and post-thrombotic iliac vein obstruction," *European Journal of Vascular and Endovascular Surgery*, vol. 20, no. 6, pp. 560–571, 2000.